European Journal of Medicinal Chemistry 266 (2024) 116094

Contents lists available at ScienceDirect

European Journal of Medicinal Chemistry

journal homepage: www.elsevier.com/locate/ejmech

Research paper

Aminoquinoline-based Re(I) tricarbonyl complexes: Insights into their antiproliferative activity and mechanisms of action

Paige S. Zinman [a], Athi Welsh [a], Reinner O. Omondi [a], Saif Khan [b], Sharon Prince [b], Ebbe Nordlander [c], Gregory S. Smith [a,*]

[a] Department of Chemistry, University of Cape Town, Rondebosch, 7701, South Africa
[b] Department of Human Biology, University of Cape Town, Faculty of Health Science, Observatory, 7925, South Africa
[c] Chemical Physics, Department of Chemistry, Lund University, Box 124, SE-221 00, Lund, Sweden

ARTICLE INFO

Keywords:
Rhenium(I)
Aminoquinoline
Cytotoxicity
DNA/BSA binding
Molecular docking

ABSTRACT

In an effort to develop new potent anticancer agents, two Schiff base rhenium(I) tricarbonyl complexes, containing the ubiquitous aminoquinoline scaffold, were synthesized. Both aminoquinoline ligands and Re(I) complexes showed adequate stability over a 48-h incubation period. Furthermore, the cytotoxic activity of the precursor ligands and rhenium(I) complexes were evaluated against the hormone-dependent MCF-7 and hormone-independent triple negative MDA-MB-231 breast cancer cell lines. Inclusion of the $[Re(CO)_3Cl]^+$ entity significantly enhanced the cytotoxicity of the aminoquinoline Schiff base ligands against the tested cancer cell lines. Remarkably, the incorporation of the Schiff-base iminoquinolyl entity notably enhanced the cytotoxic activity of the Re(I) complexes, in comparison with the iminopyridyl entity. Notably, the quinolyl-substituted complex showed up to three-fold higher activity than cisplatin against breast cancer cell lines, underpinning the significance of the quinoline pharmacophore in rational drug design. In addition, the most active Re(I) complex showed better selectivity towards the breast cancer cells over non-tumorigenic FG-0 cells. Western blotting revealed that the complexes increased levels of γH2AX, a key DNA damage response protein. Moreover, apoptosis was confirmed in both cell lines due to the detection of cleaved PARP. The complexes show favourable binding affinities towards both calf thymus DNA (CT-DNA), and bovine serum albumin (BSA), and the order of their interactions align with their cytotoxic effects. The *in silico* molecular simulations of the complexes were also performed with CT-DNA and BSA targets.

1. Introduction

Despite numerous clinical successes and innovative research breakthroughs, the incidence of cancer continues to increase worldwide. Breast cancer is the most frequently diagnosed form of cancer, globally, accounting for 1 in 8 cancer diagnoses across both sexes [1,2]. Furthermore, it is the second leading cause of death due to cancer in women, particularly burdening those living in developing countries [1–3]. There is a dire need for new and improved cancer chemotherapeutic agents, ones that possess unique mechanisms of action, have superior selectivity, are less toxic, and can withstand chemoresistance [4].

Schiff-base ligands [5–7] are renowned for being privileged scaffolds in the drug design of robust drug candidates owing to their facile synthesis, favourable denticity for chelation, and the relatively simple tuning of their electronic and steric properties [8–10]. Schiff base molecules have shown pertinence in a range of applications and industries, from analytical chemistry [11] to catalysis [9] and biomedical applications [11–14], with their notable biological activity attributed to the characteristic imine –C═N functionality [15]. Numerous reports highlight the versatility of Schiff base metallodrugs, showcasing substantial anticancer properties [16–20], and demonstrating effectiveness as antibacterial [21–23], antifungal [24–26], and antiparasitic agents [15,17,27]. These attributes have earned them recognition as 'privileged scaffolds' [10]. The following metal Schiff base complexes, exemplifying potent biological activity, highlight their dominance in medicinal chemistry research. Garza-Oritz et al. demonstrated Ru(II)-bis(arylimino)pyridine complexes' potent anticancer activity against seven cancer cell lines [28]. Suárez-Oritz *et al.* reported selective cytotoxicity of chiral *fac*-tricarbonyl(iminopyridine) rhenium(I) complexes

* Corresponding author.
E-mail address: gregory.smith@uct.ac.za (G.S. Smith).

https://doi.org/10.1016/j.ejmech.2023.116094
Received 13 October 2023; Received in revised form 13 December 2023; Accepted 21 December 2023
Available online 27 December 2023

against glioblastoma cells [20]. Bulatov *et al.* found an Isatin-Schiff base-copper(II) complex inhibiting p53-positive MCF-7 cell proliferation, activating p53, and inducing apoptosis [29]. A series of Ru (II)-arene Schiff base complexes exhibited low micromolar anticancer activity *via* a p53-independent pathway against colorectal and gastric cancer cell lines [30]. Novicidin attached to a zinc-Schiff base carrier effectively penetrated prostate PC3 cancer cells, suggesting its potential as a novel anticancer drug [31].

The aminoquinoline structure in itself is also a versatile and ubiquitously bioactive scaffold. This structural motif is present in a variety of biologically active molecules and displays activity against a myriad of human diseases [32]. This is best exemplified by the clinical malaria drug, chloroquine [33]. Other than malaria, chloroquine has also been utilized to treat several autoimmune diseases including systemic lupus, erythematosus and rheumatoid arthritis [34,35]. More recently, quinoline-based drugs, such as chloroquine, have been studied for cancer treatment [36,37]. As a pivotal pharmacophoric scaffold, the incorporation of the quinoline structure constitutes a well-founded rationale for the design and synthesis of more selective anticancer agents [32]. Interestingly, recent research reveals that this nitrogen heterocycle induces anticancer effects by intercalating between DNA base pairs or disrupting proteins that regulate DNA structure and cell proliferation [32]. For example, a recurrent scaffold in intercalating agents is amsacrine, a quinoline-containing molecule, and one of the first DNA intercalators investigated and used to treat blood malignancy [32,38].

With the pivotal discovery of the platinum-based anticancer drug, cisplatin [39], the hybridization of bioactive organic moieties with metals is documented to display significant pharmacological advantages and is a prevalent strategy in rational drug design of novel chemotherapeutics [40,41]. Transition metal complexes have been used to improve many traditional organic-based medical treatments by enhancing the bioavailability of drugs through increased lipophilicity, effectively inhibiting enzymes, functioning as biocatalysts through reversible redox behaviour and decreasing the required dosage for effective treatment [41–45]. Even with the widespread success of platinum-based anticancer drugs, many serious clinical limitations have developed which signify a poor patient prognosis [46–49], leading to the ever-current exploration for alternative metal-based anticancer agents [50]. Ruthenium, titanium and gold anticancer agents have been at the forefront of research efforts, revealing extremely promising results with some complexes progressing to phase I and II clinical trials [42,51,52]. These advances propelled the investigations into metals further down the Periodic Table such as the third-row transition metals of iridium, osmium and rhenium which have been found to also exhibit encouraging anticancer properties [43,46,53]. Relatively unexplored, rhenium-based complexes with the stable rhenium(I) tricarbonyl motif exhibit promising features for designing theranostic (therapeutic and diagnostic) agents due to their compact size compared to larger polypyridyl complexes, kinetic stability, easy modular synthesis, and rich spectroscopic properties [46,54]. In fact, various Re(I) tricarbonyl complexes, some of which encompass a quinoline moiety (Fig. 1), have already emerged to display notable cytotoxic activity against a range of cancerous cell lines [24,46,54–61]. Despite the promising potency demonstrated by rhenium(I) complexes, there has been limited research into elucidating their mechanism of action and further investigations are highly warranted [46,62].

The study reported herein, endeavoured to develop 4-aminoquinoline Schiff base ligands and their corresponding *N,N*-chelated rhenium (I) tricarbonyl complexes. The synthesized compounds were evaluated *in vitro* as potential anticancer drug leads against the hormone-dependent MCF-7 and hormone-independent MDA-MB-231 breast cancer cell lines. In addition, the selective cytotoxicity of the complexes was assessed against the non-malignant dermal fibroblast cell line, FG-0. To gain further insight into the complexes' possible mechanism of action, this study investigated their effect on the expression of key molecular markers associated with DNA damage and apoptosis. Furthermore, the interactions of the rhenium complexes with biomolecules such as calf thymus DNA (CT-DNA) and bovine serum albumin (BSA) was evaluated through spectroscopic and *in silico* methods.

2. Results and discussion

2.1. Synthesis and characterization

The 4-aminoquinoline Schiff base ligands **2** and **3** were synthesized *via* two steps (Scheme 1), initially involving a nucleophilic aromatic substitution (S_NAr) reaction with 4,7-dichloroquinoline and 1,3-diaminopropane to synthesize N^1-(7-chloroquinolin-4-yl)propane-1,3-diamine (**1**) [63].

The second step, following an amended literature method, involved reacting compound **1** with an aromatic aldehyde *via* a Schiff base condensation reaction [64]. Compound **2**, encompassing the iminopyridyl substituent, has been synthesized previously by Maurya et al. [64], while the quinolyl-substituted compound **3** has not been previously reported, at the time of writing. The selected aromatic aldehydes, 2-pyridinecarboxaldehyde and 2-quinolinecarboxaldehyde, were chosen to investigate the effect of an extended π-system. Furthermore, the presence of a second quinolyl entity was intended to ascertain the resulting effects on the overall biological activity of the compounds. Overall, the facile synthesis of the ligands afforded light brown **(2)** or light yellow **(3)** powders in yields of 51% and 70%, respectively.

The synthesis of the new neutral *N,N*-chelated rhenium(I) tricarbonyl aminoquinoline Schiff base complexes **4** and **5** was achieved *via* a simple ligand substitution reaction (Scheme 1) [65]. The complexes, **4** and **5**, were purified via recrystallisation and isolated as orange

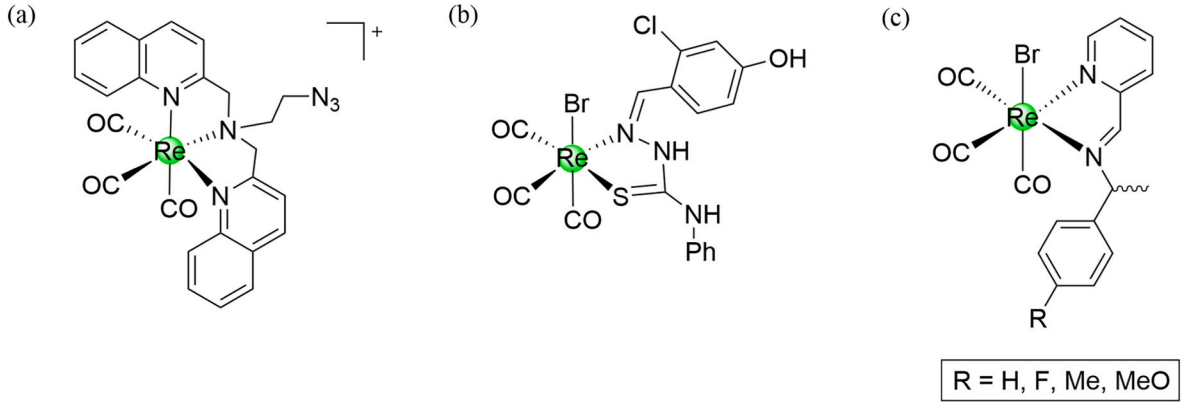

Fig. 1. Selected chemical structures of Re(I) tricarbonyl complexes with reported anticancer activity [24,55,56].

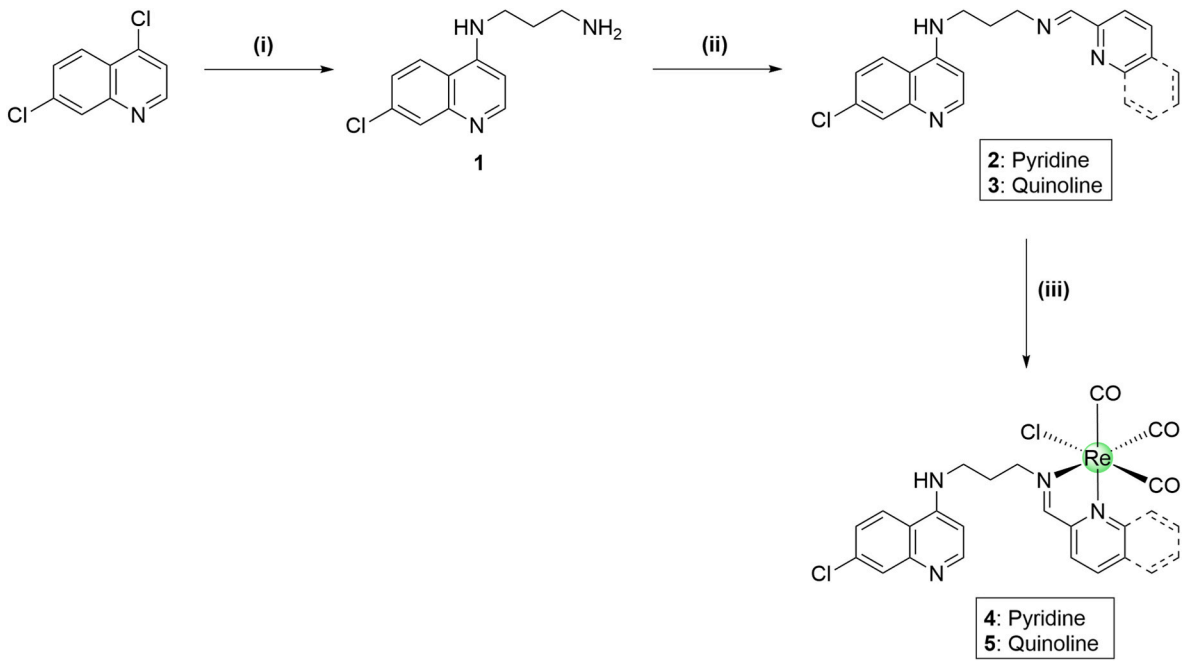

Scheme 1. Synthetic procedure of the 4-aminoquinoline precursor **1**, the Schiff base ligands (**2**–**3**) and the corresponding *N,N*-chelated Re(I) complexes **4** and **5**. Reagents and conditions: (i) 1,3-diaminopropane, 120–130 °C, 6–8 h; (ii) Aromatic aldehyde, MeOH, molecular sieves, 60 °C, 48 h; (iii) $[Re(CO)_5Cl]$ (1.1 eq.), MeOH, reflux in the dark, 18 h.

powders in yields of 68% and 59%, respectively. Both complexes are air- and moisture-stable as well as soluble in a range of polar and alcohol-based solvents. Light exposure was minimized during the synthetic procedure and the complexes were stored in the dark to prevent potential light sensitivity and the release of carbon monoxide molecules, as has been reported for analogous Re(I) tricarbonyl complexes [66–68]. The rhenium(I) tricarbonyl complexes **4** and **5** were used for *in vitro* biological evaluations as racemic mixtures.

The 4-aminoquinoline Schiff base ligands (**2** and **3)** and the corresponding Re(I) complexes (**4** and **5)** were all characterized in solution using ^{1}H, $^{13}C\{^{1}H\}$, COSY, HSQC and HMBC NMR spectroscopy, together with FT-IR spectroscopy and high-resolution electrospray ionisation mass spectrometry (ESI-MS). The spectra obtained from these characterization and analyses techniques are displayed in the Supplementary Information. ^{1}H NMR spectroscopy (Figs. S1 and S2) revealed singlets at 8.42 ppm (**2**) and 8.59 ppm (**3**) corresponding to the imine hydrogen (H_n), which attests to the formation of the respective C═N bonds of these Schiff base compounds. Further, the ^{1}H and $^{13}C\{^{1}H\}$ NMR analyses of the Re(I) complexes (**4** and **5**) confirmed successful bidentate coordination to the imine and aromatic nitrogen atoms of ligands **2** and **3** (Figs. S1–S6). Fig. S1 depicts the stacked ^{1}H NMR spectra of the pyridyl-substituted Schiff base ligand, **2**, and the respective Re(I) complex, **4**. In spectrum (b) of Re(I) complex **4**, a downfield shift of most of the aromatic and aliphatic signals is observed, with respect to that in spectrum (a) of the corresponding ligand, **2**, indicative of metal complexation. The most significant downfield shifts are seen for the proton signal H_s from 8.65 ppm to 9.10 ppm and proton signal H_n from 8.42 ppm to 9.33 ppm. This observation substantiates a bidentate coordination to the imine and the pyridyl nitrogen atoms of the ligand **2**, as the hydrogens most affected after complexation (H_s and H_n) are, indeed, those closest to the expected sites of coordination. Further evidence of complexation is the splitting of the aliphatic proton signals corresponding to the propylene hydrogen atom (H_l) of the propyl chain. The single multiplet, integrating for two hydrogen atoms, in the range 2.29–2.11 ppm in the spectrum (a) of ligand **2**, appears as two multiplets (2.64–2.48 ppm) each integrating for one proton in the spectrum (b) of complex **4**. This phenomenon has been confirmed by HSQC NMR spectroscopy (Fig. S7), i.e., the two multiplet proton signals correlate to one carbon peak. The splitting of this aliphatic signal is due to the chirality induced by the introduction of a metal-based stereogenic centre, causing the hydrogen atoms to become diastereotopic, i.e., magnetically inequivalent.

The FT-IR spectra of ligands **2** and **3** depict further evidence for the formation of the desired Schiff base ligands owing to the characteristic FT-IR absorption bands of the imine functionality ν(C═N) observed at 1581 cm^{-1} (for **2**) and at 1572 cm^{-1} (for **3**) (Figs. S8–S9). The observed absorption bands and associated wavenumbers in the FT-IR spectra of ligands **2** and **3** agree well with those reported in the literature for similarly structured compounds [69–71]. In the FT-IR spectrum of complex **4** (Fig. S8), the $\nu(C{=}N)_{imine}$ and $\nu(C{=}N)_{pyridyl}$ stretching vibrations are observed as overlapping absorption bands at 1573 cm^{-1}, agreeing with that reported in literature for other Re(I) tricarbonyl diimine complexes [72,73]. The $\nu(C{=}N)_{imine}$ stretching frequencies of complex **4** is observed at a lower wavenumber than that of the uncoordinated ligand **2**, being at 1581 cm^{-1}, while the $\nu(C{=}N)_{pyridyl}$ absorption band of complex **4** appears at a higher wavenumber than that of ligand **2** (1564 cm^{-1}). This phenomenon is, in fact, commonly reported for diimine Re(I) complexes [72,73], and is indicative of successful bidentate coordination of the imine and pyridyl nitrogen atoms to the metal. Additional evidence of complexation is seen by the appearance of three strong ν(C═O) absorption bands in the range 2014–1862 cm^{-1}, which are absent in the spectrum of the corresponding ligand, **2**. These absorption frequencies, attributed to the three carbonyl ligands bonded to rhenium, are consistent with literature reports for similarly structured Re(I) complexes [24,72,74]. In addition, the appearance of the three strong carbonyl absorption bands also suggests a *facial* arrangement of these ligands around the Re(I) metal centre.

High-resolution ESI-MS data was obtained for the ligands (**2** and **3**) and the corresponding Re(I) complexes (**4** and **5**). A base peak corresponding to the protonated molecular ion $[M+H]^+$ is observed in the spectrum for ligand **2** (Fig. S10). The positive-ion mode mass spectrum for ligand **3** shows a base peak indicative of the cationic fragment $[M+Na]^+$ (Fig. S11). Lastly, the most abundant peak in the ESI mass spectra of Re(I) complexes **4** and **5** correlate with the protonated molecular ion peak, i.e., $[M+H]^+$ (Figs. S12–S13).

The UV–Vis absorption spectra of Re(I) complexes **4** and **5**, in DMSO, are shown in Fig. 2. The intense absorption bands in the UV region at *ca.* 250–330 nm are attributed to the spin-allowed $\pi_L \rightarrow \pi_L^*$ intraligand transitions of the diimine ligands. The broader lower energy peaks at *ca.* 330–460 nm can most likely be assigned to the spin-allowed metal-to-ligand charge-transfer (^{1}MLCT) absorptions, representative of the transitions from the *d*-orbitals of the Re(I) metal to the π* orbitals of the respective diimine Schiff base ligands [75–79]. However, further detailed spectrophotometric analysis and molecular modelling studies would need to substantiate and confirm this postulation. The obtained electronic absorption spectra (Fig. 2) are comparable to those of similarly structured diimine Re(I) tricarbonyl complexes reported in the literature [80–82]. Interestingly, a slight red shift of approximately 35 nm is observed in the electronic absorbance spectrum of the quinolyl-substituted complex **5** relative to the pyridyl-substituted complex **4**, suggesting that the extended conjugated π-system of the quinolyl versus the pyridyl entity influences the wavelength at which the ^{1}MLCT band appears.

The extended π-system of the quinolyl substituent **5** slightly lowers the antibonding π* orbital of the diimine ligand, which, in turn, decreases the energy gap between the HOMO that is based on the metal *d*-orbital and the LUMO, which is a ligand π* orbital. As a result, the energy required to effect electron promotion from the metal *d*-orbital to the ligand π* orbital is lowered, resulting in a bathochromic shift of the absorption band [83].

2.2. Molecular structure of compounds *2* and *4*

The molecular structures of the pyridyl-substituted Schiff base ligand **2** and its corresponding Re(I) tricarbonyl complex **4** were elucidated by single crystal X-ray diffraction (Fig. 3). Single crystals of ligand **2** and complex **4** were grown by layering diethyl ether over a concentrated solution of either compound in dichloromethane. Complex **4** was kept in the dark, to avoid light exposure.

From the ORTEP diagram of complex **4** (Fig. 3), it is evident that the carbonyl ligands adopt a *facial* arrangement around the metal centre. This supports and agrees with the appearance of the three strong carbonyl absorption bands in the corresponding FT-IR spectrum (Fig. S8). The adoption of the *fac*-isomeric structure is commonly observed in other Re(I) tricarbonyl diimine complexes reported in literature [24,73,74,84]. The diagram also depicts coordination of a chlorine atom and the two nitrogen atoms (pyridine-N and imine-N) of ligand **2** to the Re(I) metal ion. Moreover, noticeable disorder is observed at Cl1, C21 and O3, with a site occupancy factor (S.O.F.) of <0.1. The apparent disorder is owing to the co-crystallisation of more than one isomer, resulting in a crystallographic structure that is an overlay and average of all the asymmetric units present. Table S2 summarises the crystal data and refinement parameters for both ligand **2** and complex **4**. Ligand **2** crystallizes in a P-1 space group with a triclinic system, while complex **4** crystallizes in a $P2_1/c$ space group with a monoclinic system. A total of two and four molecules per unit cell are observed for ligand **2** and complex **4**, respectively.

Selected bond distances and angles for both compounds are listed in Table S3. Complex **4** adopts a distorted octahedral geometry around the rhenium metal ion. The deviation of the rhenium coordination sphere from the ideal octahedron is due to the compression brought about by the five-membered chelate ring (Re1-N1-C13-C14-N4), leading to a small bite angle of 74.88(8)°. The observed bond angles and resulting geometry around the Re(I) metal centre are comparable with other Re(I) tricarbonyl diimine complexes reported in literature [50,72,84]. The Re-$N_{pyridyl}$ bond length, Re1-N4, 2.170(2) Å is almost equivalent to the Re-N_{imine}, Re1-N1, bond length of 2.175(2) Å, which is corroborated by the FT-IR data collected (Fig. S8), where the ν(C═N)$_{pyridyl}$ and ν(C═N)$_{imine}$ are seen to be overlapping and resonating at very similar frequencies. In fact, these bonding parameters are consistent with that reported in literature for structurally similar *N,N*-Re(I) tricarbonyl complexes [50,72]. Additionally, the C=N_{imine} bond of complex **4**, C13–N1, 1.274(3) Å is slightly longer than that of the respective ligand **2**, C13–N13, 1.264(2) Å, which is expected due to the Re (d-π) – imine (π*) backdonation. This observation is also corroborated by the FT-IR spectrum (Fig. S8) where there is a small shift in the ν(C═N)$_{imine}$

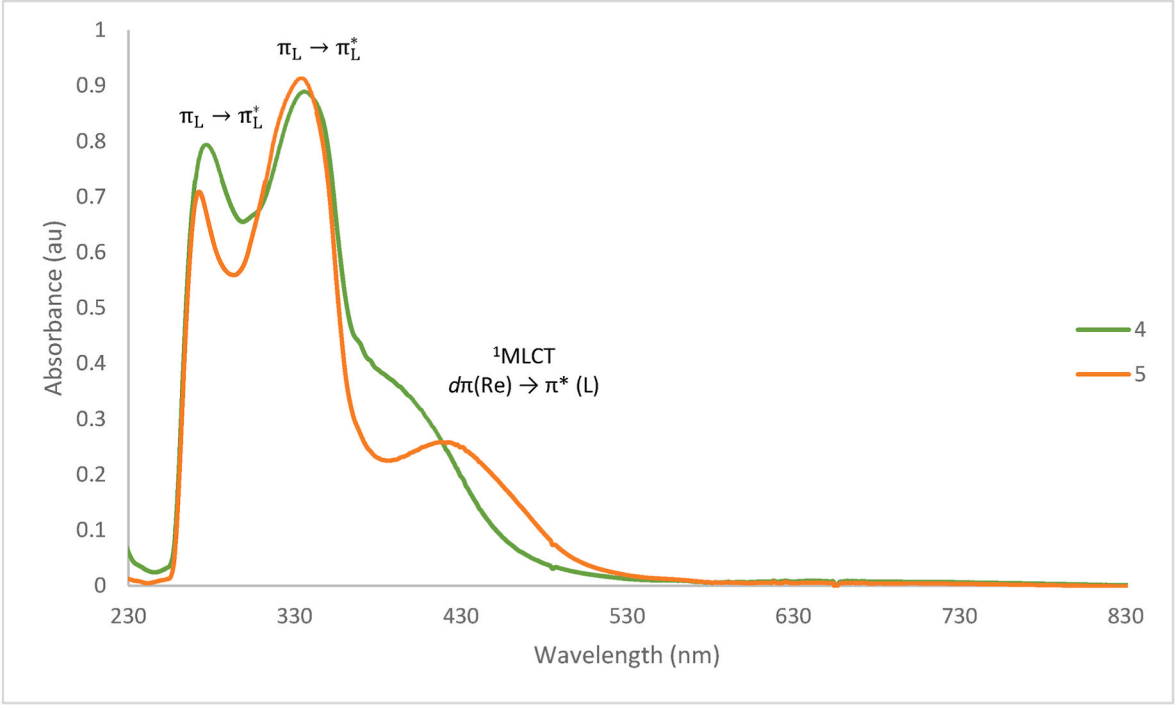

Fig. 2. Stacked UV–Vis absorption spectra of Re(I) complexes **4** (green) and **5** (orange) measured in DMSO at concentrations of *ca.* 1×10^{-4} M and *ca.* 0.5×10^{-4} M, respectively, under ambient conditions.

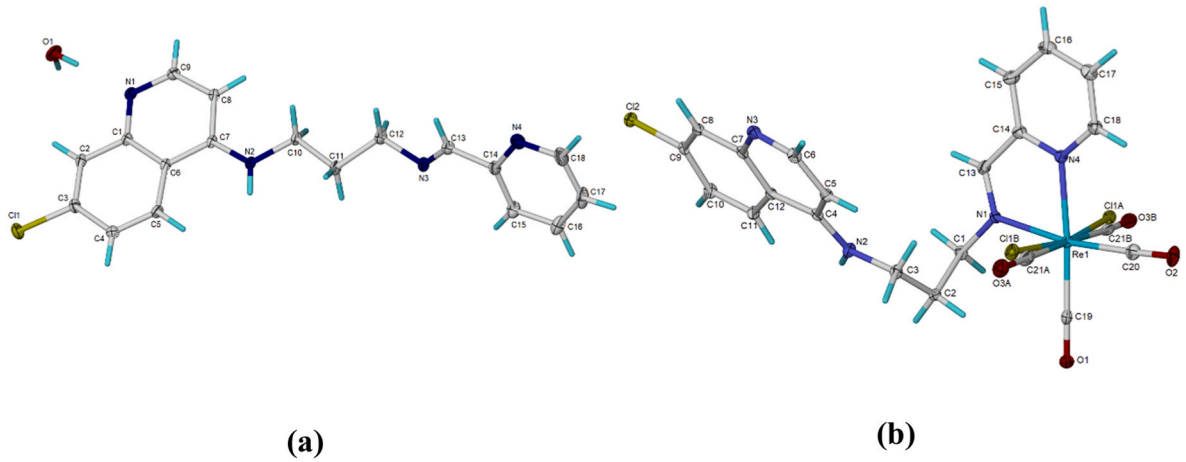

Fig. 3. ORTEP diagrams of (a) 4-aminoquinoline pyridyl-substituted Schiff base ligand **2** and (b) Re(I) tricarbonyl *N,N*-chelated complex **4**, with hydrogen atoms omitted from both structures for clarity. Thermal ellipsoids are drawn at 30% probability level for both structures.

absorption band from a higher wavenumber, for ligand **2**, to a lower wavenumber, for the complex **4**. For complex **4**, the new 5-membered ring formed by chelation is essentially planar with a torsion angle of −1.1(4)°, which has been commonly observed for closely related complexes in literature [85]. In the case of the uncoordinated ligand, **2**, the pyridyl and imine functionalities are not co-planar, but rotated 172.69° from each other, as has been noted for similarly structured Schiff base compounds [86]. Furthermore, the Re-Cl, Re-$C_{carbonyl}$ and C-$O_{carbonyl}$ bond distances of complex **4** are within the expected range as reported in literature for this class of Re(I) complex [72,73,84].

2.3. Solution stability studies

Metal-based complexes have, in the past, been known to show instability under physiological conditions, leading to undesirable side effects [87–89]. The stability of a compound is a crucial factor in the classification and discernment of viable drug leads for biological applications. Stability studies commonly involve the use of DMSO, which is arguably the most frequently used organic solvent for *in vitro* biological screenings of compounds [90]. There have been reports that cisplatin and related platinum-based complexes (carboplatin and oxaliplatin) undergo ligand displacement when dissolved in DMSO, due to the affinity of the Pt(II) centre for the nucleophilic sulfur donor atom of DMSO [91,92]. For the biological studies to be relevant, the stability of the aminoquinoline Schiff base ligands **2** and **3** and Re(I) complexes **4** and **5** was monitored using UV–Vis spectroscopy. Complexes **4** and **5** were dissolved in PBS supplemented with 1% DMSO and the absorption spectra were recorded over 48 h, while maintaining the physiological temperature of 37 °C. The testing conditions mimicked the environment of the *in vitro* cytotoxicity screenings (*vide infra*).

The obtained temporal UV–Vis spectra of the complexes **4** and **5** are shown in Fig. 4. The complexes showed negligible changes in the electronic bands, pointing to their stability. Additionally, no considerable changes in the absorption spectra of ligands **2** and **3** were observed in DMSO over 48 h (Fig. S14) signifying their stability and structural integrity. This is pertinent, as the compounds are incubated with the cancer cell lines for precisely 48 h during the *in vitro* biological assays.

2.4. In vitro cytotoxicity evaluation

The cytotoxic activity of the aminoquinoline Schiff base ligands **2** and **3** and the corresponding *N,N*-mononuclear complexes **4** and **5** were assessed against two breast cancer cell lines (MCF-7 and MDA-MB-231) and a non-tumorigenic cell line (FG-0). The compounds were pre-

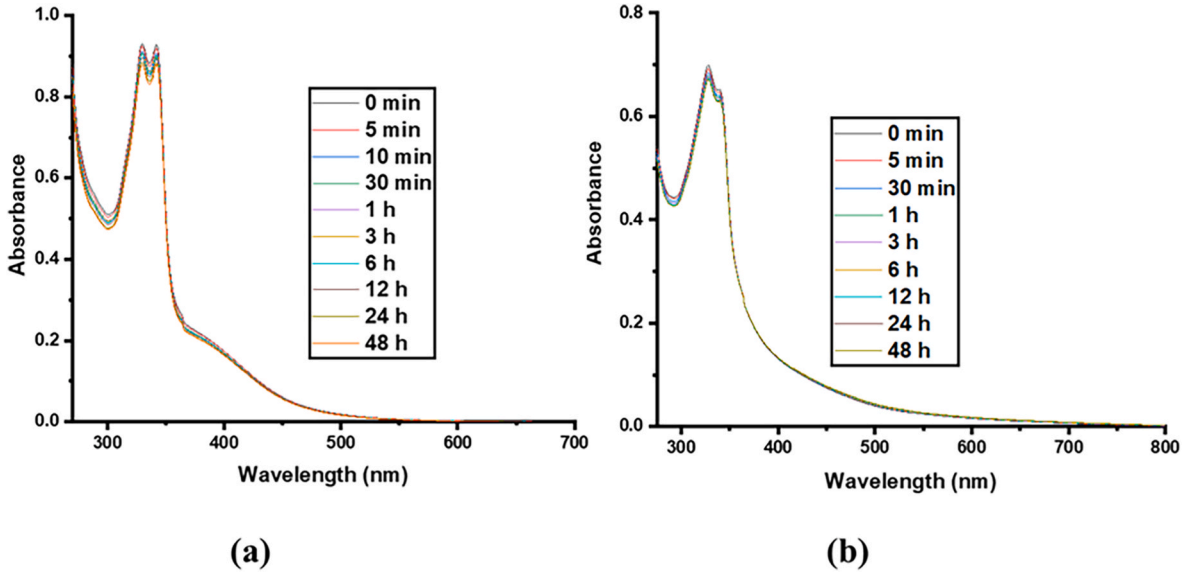

Fig. 4. The temporal UV–Vis spectra of (a) iminopyridyl Re(I) complex **4** and (b) iminoquinolyl Re(I) complex **5** in PBS (with 1% DMSO) at 37 °C for 48 h.

screened *in vitro* against the hormone-dependent MCF-7 and hormone-independent MDA-MB-231 cell lines at 10 μM and 20 μM using the MTT (3-(4,5-dimethylthiazol-2-yl)-2,5-diphenyltetrazolium bromide) assay [93]. In all assays performed, DMSO was used as the biological vehicle; therefore, it was included as a negative control when diluted in growth medium (0.1% DMSO in growth medium). Additionally, a clinically used chemotherapeutic metallodrug, cisplatin, was included as the positive control and for comparison purposes.

The percentage cell viability of MCF-7 cells following treatment with the aminoquinoline Schiff base ligands (**2, 3**) and the corresponding Re (I) tricarbonyl complexes (**4, 5**) is herein represented in Fig. 5. Overall, the ligands and complexes all show moderate to good activity against this cell line, at both tested concentrations. At 10 μM, the compounds **2**–**5** reduce cell viability by between 38% and 80% while at 20 μM the cell viability is further reduced by 42%–94%. Therefore, these compounds generally show activity in a dose-dependent manner, i.e. there is an enhancement of cytotoxicity upon doubling the compound concentration from 10 μM to 20 μM. Moreover, the tested ligands and complexes show superior cytotoxic activity in comparison with cisplatin at both tested concentrations in the MCF-7 breast cancer cell line.

Notably, the introduction of the rhenium(I) ion appears to enhance the biological activity of the ligands, **2** and **3**, as seen by the comparably lower percentage cell viability of the respective Re(I) tricarbonyl complexes, **4** and **5**. For example, complex **5** inhibits the cell viability by 34% (at 10 μM) and 42% (at 20 μM), more than the corresponding ligand **3**. In fact, the quinolyl-substituted complex **5** is the most active compound boasting a 20% and 6% cell survival at 10 μM and 20 μM, respectively. This remarkable cytotoxic activity is likely attributed to the presence of the additional quinolyl entity. Comparatively, its analogue, the pyridyl-substituted complex **4**, shows a lower potency, reducing cell survival to 52% (at 10 μM) and 36% (at 20 μM). A similar observation is made between the pyridyl-substituted ligand **2** and the quinolyl-substituted ligand **3**, where there is a clear improvement in cytotoxic activity upon incorporation of the quinolyl moiety ligand **3** over the pyridyl moiety ligand **2**. At 10 μM, the quinolyl-substituted ligand **3** reduced cell survival by 46%, while the pyridyl-substituted ligand **2** reduced cell survival by only 38%. This observation highlights the ubiquitous pharmacological activity of the quinoline structure, suggesting that the presence of the iminoquinolyl motif, in addition to the 4-aminoquinoline core, positively influences the cytotoxic activity of tested compounds, **3** and **5**.

The MDA-MB-231 breast cancer cell line is a triple-negative cancer cell subtype, which lacks the oestrogen, progesterone, and human epidermal growth factor 2 hormone receptors [94,95]. This cell line represents a highly invasive form of breast cancer that is notoriously difficult to treat [95]. The data obtained from the cytotoxic evaluation of the ligands (**2, 3**) and corresponding *N,N*-complexes (**4, 5**) against the MDA-MB-231 cell line, at 10 μM and 20 μM, is shown in Fig. 6.

The preliminary cytotoxicity data for the compounds, against the MDA-MB-231 cell line, somewhat resembles the trends observed for the MCF-7 cell line (Fig. 5). The ligands **2** and **3** and Re(I) complexes **4** and **5**, again, show activity in a dose-dependent manner and, in fact, inhibit cell viability to a greater extent than cisplatin, 12% (10 μM) and 36% (20 μM). Comparatively, the Re(I) complexes, **4** and **5**, exhibit superior activity relative to the uncoordinated ligands **2** and **3**, with cell viability inhibitions of 42% and 60%, at 10 μM, and 70% and 98%, at 20 μM, respectively. This phenomenon reiterates the beneficial role of transition metal complexes in giving rise to effective medical treatments for critical human diseases. Furthermore, the results highlight the promising anticancer properties of the rhenium(I) tricarbonyl core.

Owing to the promising activity in the pre-screen assays the *N,N*-chelated Re(I) complexes (**4,5**) were selected for further *in vitro* multi-dose screenings against the two breast cancer cell lines (MCF-7 and MDA-MB-231) and a non-tumorigenic cell line (FG-0) to further ascertain their potential as therapeutic agents. The concentrations of complexes **4** and **5** required to reduce cell viability to 50% of the control (IC_{50}) are summarized in Table 1. In these experiments, the relevant cancer cells were treated with the test compounds (**4, 5**) over a range of concentrations from 0 μM to 35 μM for 48 h and the cell viability was measured using the MTT assay. For comparison, cisplatin was included as a positive control and a 0.1% DMSO in cell culture media solution was included as a negative control. Furthermore, the experiments were conducted in the dark, with limited white light exposure, for the entire duration of the assay.

As observed from the pre-screen data, the Re(I) complexes (**4, 5**) display a dose-dependent cytotoxic activity against the MCF-7 breast cancer cell line (Fig. S15). Both complexes **4** and **5** display enhanced cytotoxicity relative to clinically used cisplatin in this cancer cell line. Impressively, complex **5** displays up to 3.6 times greater activity relative to cisplatin (IC_{50} = 24.92 μM). From the results, it is apparent that the complexes **4** and **5** show statistically comparable cytotoxicity with an IC_{50} value of 6.82 ± 1.03 μM for the quinolyl-substituted Re(I) complex,

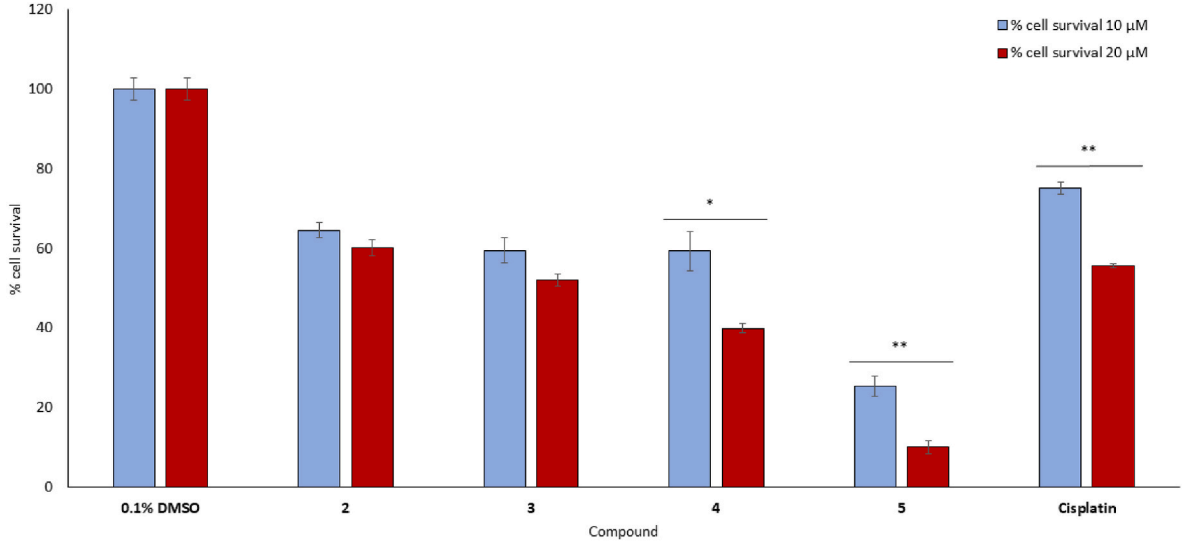

Fig. 5. *In vitro* cytotoxic effect of aminoquinoline Schiff base ligands (**2, 3**) and corresponding *N,N*-bidentate Re(I) complexes (**4, 5**) towards the MCF-7 breast cancer cell line at 10 μM and 20 μM. Results displayed as the percentage cell survival as measured by MTT assays, cisplatin and the vehicle (0.1% DMSO) are included as controls. * = $p \leq 0.05$, thus statistically significant and ** = $p \leq 0.01$, thus very statistically significant.

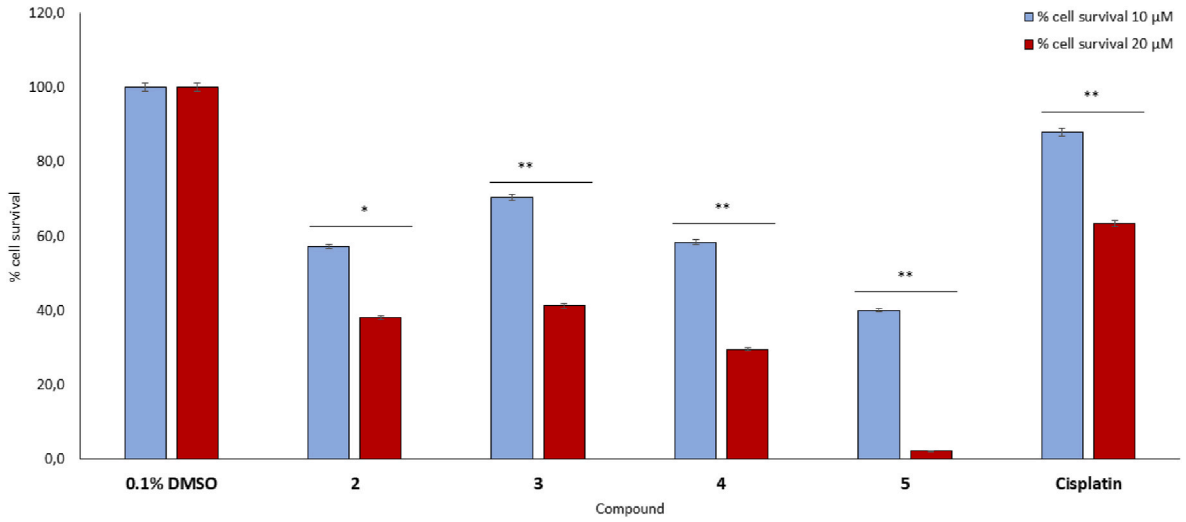

Fig. 6. *In vitro* cytotoxic effect of aminoquinoline Schiff base ligands (**2, 3**) and corresponding *N,N*-bidentate Re(I) complexes (**4, 5**) towards the MDA-MB-231 breast cancer cell line at 10 μM and 20 μM. Results displayed as the percentage cell survival as measured by MTT assays, cisplatin and the vehicle (0.1% DMSO) are included as controls. * = $p \leq 0.05$, thus statistically significant and ** = $p \leq 0.01$, thus very statistically significant.

Table 1
IC_{50} values of the Re(I) complexes (**4**, **5**) against two breast cancer cell lines (MCF-7 and MDA-MB-231) and a non-tumorigenic cell line (FG-0). [a]

Compound	IC_{50} (μM)			S.I.
	MCF-7	MDA-MB-231	FG-0	
4	8.55 ± 1.08	17.70 ± 0.75	7.09 ± 0.17	0.83
5	6.82 ± 1.03	10.73 ± 0.53	10.86 ± 0.23	1.59
Cisplatin	24.92 ± 1.03	24.45 ± 1.03	43.67 ± 1.05*	1.75

S.I.: Selectivity Index = IC_{50} FG-0/IC_{50} MCF-7.
[a] The results are presented as mean values ± standard deviations (SD) out of two independent experiments and the cell viability was assessed after 48 h of incubation.
* IC_{50} value extrapolated by Graphpad Prism V 8.0.2 from experimental data.

5, and 8.55 ± 1.08 μM for the pyridyl-substituted analogue **4**.

A slightly different trend can be delineated for the cytotoxicity of the complexes in the MDA-MB-231 cell line to that observed in the MCF-7 cell line (Fig. S16), with the iminoquinolyl complex **5** (IC_{50} = 10.73 μM) being more cytotoxic than the iminopyridyl complex **4** (IC_{50} = 17.70 μM). However, the complexes (**4**, **5**) prove to be less potent against the aggressive triple-negative MDA-MB-231 cell line than against the MCF-7 cell line, by a factor of approximately 2 for both complexes. Nevertheless, this observation is noteworthy in that it shows that the compounds must have a well-defined mechanism of action and are not simply broad-spectrum toxins. Intriguingly, complex **4** still shows slightly greater potency than the positive control, cisplatin (IC_{50} = 24.45 μM), while the iminoquinolyl complex **5** shows up to 2 times greater cytotoxicity than the clinical metallodrug. Once again, this observation emphasizes that the addition of the second quinolyl entity to the aminoquinoline Schiff base ligand in complex **5** evidently enhances the cytotoxic activity of the rhenium(I) complex against the breast cancer cell line. Furthermore, this suggests that the additional quinoline substituent contributes to the observed cytotoxic activity and is, itself, eliciting a cytotoxic effect on the cancer cells. However, without a detailed structure-activity based assessment, it is difficult to say whether this is an additive or synergistic effect.

Both tested complexes **4** and **5** show concentration-dependent cytotoxicity towards the non-tumorigenic FG-0 cell line (Fig. S17). Pyridyl-substituted complex **4** shows enhanced cytotoxicity relative to quinolyl-substituted complex **5** and, overall, cisplatin is noted to show milder cytotoxicity relative to both tested Re(I) complexes. The selectivity indices summarized in Table 1 show that complex **5** which is overall more active against the breast cell lines is also the most selective, with an S.I. that is greater than 1. This indicates that complex **5** shows selective cytotoxicity towards the breast cancer cells over non-tumorigenic cells.

2.5. Western blot analysis

In a bid to gain insight on the potential mechanism of action of complexes **4** and **5** in the breast cancer cell lines (MCF-7 and MDA-MB-231), Western blotting was used to investigate the ability of the complexes to elicit DNA damage and apoptosis. This was achieved by assessing the protein levels of key markers of DNA damage and apoptosis, γH2AX and cleaved PARP, respectively. γH2AX is a central biomarker of double-strand DNA breaks, while the cleavage of PARP during apoptosis is a key hallmark of this type of cell death [96,97]. As such, DNA damage and apoptosis are indicated by increased protein levels of γH2AX and cleaved PARP.

The data obtained from Western blotting experiments are summarized in Fig. 7, below. Generally, addition of complexes **4** or **5** does indeed result in double-strand DNA breaks and significant DNA damage in both the MCF-7 and MDA-MB-231 breast cancer cell lines. This is evidenced by the notable increase in γH2AX protein levels upon treatment of the cells with complexes **4** and **5**. Furthermore, the DNA damage elicited by complexes **4** and **5** is noted to be concentration-dependent in both breast cancer cell lines, as the γH2AX protein levels of cells treated with the IC_{50} concentrations of **4** and **5** is generally higher than those treated with a lower concentration of the complexes ($^1/_2$ IC_{50}). Interestingly, complex **5** induced greater DNA damage in the MCF-7 cell line relative to the clinically used, DNA-damaging metallodrug cisplatin.

The treatment of the cells with complexes **4** and **5** resulted in a significant increase in cleaved PARP protein levels in both investigated breast cancer cell lines (MCF-7 and MDA-MB-231). This observation indicates that **4** and **5** do indeed induce apoptosis as a pathway of cell death in these breast cancer cell lines. Furthermore, the densitometric readings for cleaved PARP in both cell lines show that complex **4** may be a more potent inducer of apoptosis relative to clinically used cisplatin, as the levels of cleaved PARP in cells treated with **4** are significantly higher than those treated with cisplatin (Fig. 7). Interestingly, $^1/_2$ IC_{50} treatment of complex **5** induced greater PARP cleavage compared to IC_{50} treatment which may indicate that complex **5** induces additional forms of cell death in MCF-7 cells at this concentration. Taken altogether, these

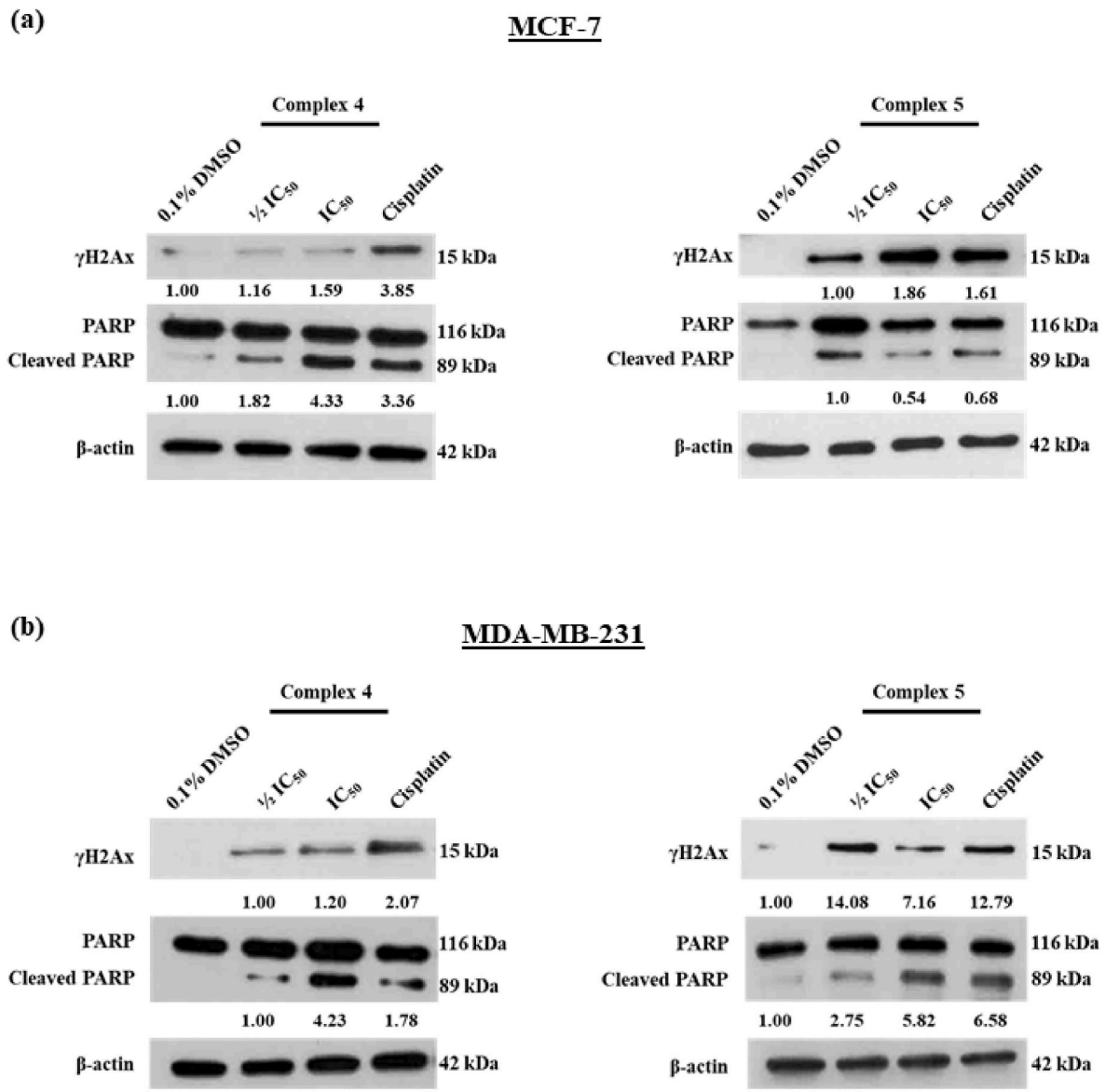

Fig. 7. Complexes **4** and **5** initiate the DNA damage and apoptosis pathways. Western blot analysis with antibodies to indicate protein levels of γH2AX, PARP and cleaved PARP in (a) MCF-7 and (b) MDA-MB-231 cells treated with ½ IC_{50} and IC_{50} of complex **4** and **5** for 48 h. β-actin was used as a loading control. Densitometry readings were obtained from three independent experiments using ImageJ and protein expression levels are represented as a ratio of protein of interest/β-actin normalized to the control sample (where possible).

mechanistic studies indicate that complexes **4** and **5** induce apoptosis through a process involving DNA damage in the investigated breast cancer cells.

2.6. DNA binding studies

2.6.1. UV–vis spectroscopy

Investigations into possible binding interactions between the Re(I) complexes (**4, 5**) and CT-DNA, as a potential mechanistic route, were conducted by absorption titration experiments. The electronic absorption spectra of CT-DNA kept at a constant concentration of 50 μM in PBS buffer solution (pH 7.2), with increasing amounts of metal complexes (0–350 μM) are given in Fig. 8. The hyperchromic effect is observed at 260 nm by consecutive addition of the metal complexes to CT-DNA. This observation suggests that the complexes specifically bind to the purine and pyridine bases of the DNA, leading to a subsequent moderate change in the conformation of DNA [98–101]. The binding constant K_b was evaluated from the ratio of the slope in the plots of $1/A\text{-}A_0$ vs 1/[metal complex] curve. The resulting binding constants for the interaction between CT-DNA and the rhenium(I) complexes (**4, 5**) are given in Table 2. The high magnitude K_b values of complexes **4** and **5** (10^4-10^5), depict intercalation with the DNA.

The order of the calculated binding constants (K_b) shows that compound **5** exhibits greater binding affinity than compound **4**, demonstrating that the additional quinolyl moiety in **5** contributes to stronger interactions with DNA in comparison to the pyridine moiety. This result follows the trend from the *in vitro* cytotoxicity experiments where the quinolyl-substituted complex **5** exhibited greater cytotoxic activity towards the cancer cell lines than the pyridyl-substituted complex **4**. This suggests that the stronger DNA interactions attributed to the quinolyl substituent may play an important role in the cytotoxic action of this rhenium complex. Notably, reports have described the structural and electronic properties of quinoline, such as its planarity and highly conjugated system, to contribute to its impressive ability to insert itself between the DNA base pairs. This action disrupts the double helix of DNA and causes strand breaks, ultimately leading to cytotoxicity [32,

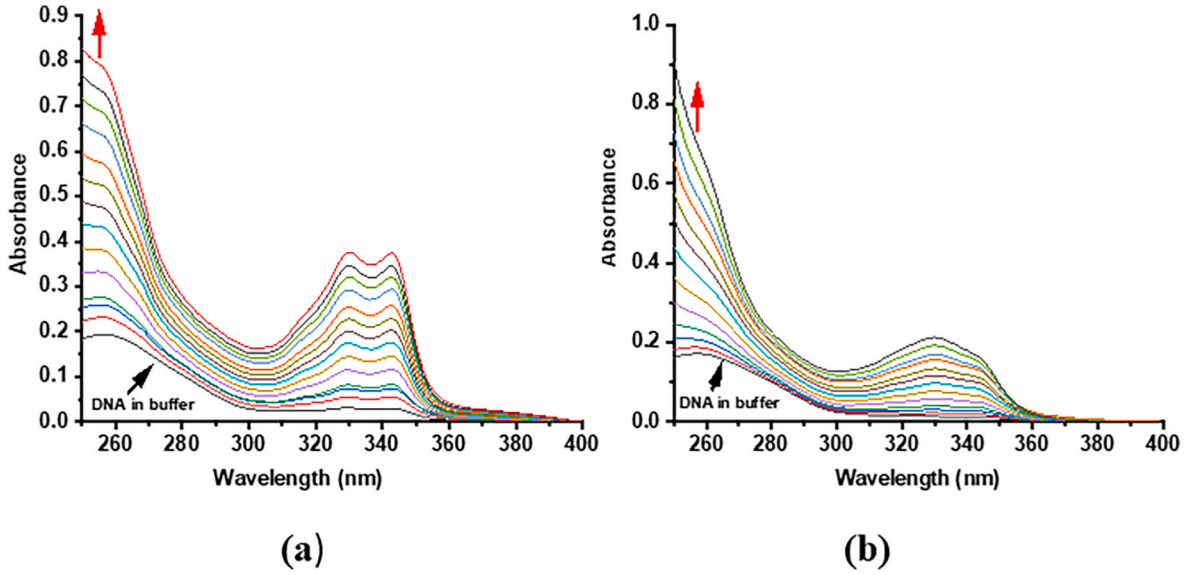

Fig. 8. Electronic absorption spectra of CT-DNA [50 μM] in the presence of increasing concentration of (a) complex **4** [0–350 μM] and (b) complex **5** [0–350 μM] in PBS buffer (pH = 7.2, 25 °C). The arrows indicate absorbance changes with the increasing concentration of metal-complexes.

Table 2
The binding and thermodynamic parameters for the interactions of complexes **4** and **5** with CT-DNA.

Compound	K_b (10^5 L.mol^{-1})	-$\Delta G^{\neq}_{25^\circ C}$ (kJ·mol^{-1})
4	0.88 ± 0.33	28.20
5	2.67 ± 0.81	30.95

102]. The positive relationship between the strength of DNA binding and the degree of anticancer activity of tested compounds has also regularly been observed and reported in the literature [61,103]. The K_b values of **4** and **5** compare well with those of similar complexes reported in the literature [103–111].

Gibb's free energy of activation (ΔG) values were derived from the van't Hoff Eq. (2) [112], as indicated in the experimental procedures and the results are presented in Table 2. The negative values for **4** and **5** signify that the interactions between the complexes and CT-DNA occur spontaneously [113].

2.6.2. *Ethidium bromide competitive studies*

To further explore and validate the mode of interactions between the rhenium complexes (**4, 5**) and CT-DNA, a fluorescent-quenching assay based on the ethidium bromide (EtBr) adduct was conducted [114–117]. Figs. 9 and 10 depict the fluorescence spectra of the CT-DNA-EtBr composite with varying concentrations (0–150 μM) of complexes **4** and **5**, respectively. The emission intensities at 600 nm show significant hypochromic shift.

These results suggest that the rhenium complexes (**4, 5**) quench the CT-DNA-EtBr fluorescence by intercalating with the DNA base pairs while simultaneously displacing the EtBr molecule (due to the decrease of the binding sites available to EtBr). The Stern-Volmer quenching constant (K_{sv}) and bimolecular quenching rate constant (kq) were determined from the Stern-Volmer Eq (3) [118], and the data are presented in Table 3.

The K_{SV} values for complexes **4** and **5** are 2.88×10^5 M^{-1} and 7.91×10^5 M^{-1}, respectively, and the magnitude of 10^5 M^{-1} indicates that the complexes can displace the EtBr bound to CT-DNA via an intercalative mode of interaction. Notably, the K_{SV} values show a striking 10^2 -fold reduction compared to the classical intercalator EtBr (10^7 M^{-1}), signifying a relatively moderate intercalative interaction [119]. The k_q values are 1.30×10^{13} M^{-1}s^{-1} and 3.04×10^{13} M^{-1}s^{-1} for complexes **4** and **5**, respectively, and are due to short-range interactions between the rhenium complexes and the CT-DNA-EtBr adduct [118]. The dynamic quenching process in various diffusion-controlled biomolecular reactions has been reported to have a maximum value of 2×10^{10} M^{-1} s^{-1} [120]. Thus, considering that the k_q values for complexes **4** and **5** exceed this limit, it may be deduced that a static mechanism is in operation [121,122]. Generally, complexes **4** and **5** exhibit K_{SV} and k_q values which are similar to related rhenium(I)-based complexes reported in the literature, implying that complexes **4** and **5** experience a relatively comparable intercalative interaction with CT-DNA [120,123,124]. In addition, the K_{SV} and k_q results indicate that the iminoquinolyl-coordinated Re(I) complex **5** binds more favourably to CT-DNA in comparison to the iminopyridyl-coordinated Re(I) complex **4**.

The apparent association constant (K_{app}), given in Table 3, was calculated for each complex (**4, 5**) using Eq. (4) [125]. For the iminopyridyl-coordinated rhenium(I) complex (**4**) K_{app} is calculated to be 5.51×10^6 M^{-1} whereas, for the iminoquinolyl-coordinated rhenium (I) complex (**5**), it is 14.06×10^6 M^{-1}. The magnitude of the K_{app} (10^6 M^{-1}) are relatively lower compared to the binding constants of classical intercalators (10^7 M^{-1}), indicating moderate intercalative interaction abilities [104].

The Scatchard Eq. (5) was applied to determine the binding constant (K_F) and the number of binding sites (n) on CT-DNA for each Re(I) complex [126]. The corresponding results are presented in Table 3. Complexes **4** and **5** display moderate quenching efficiencies, as shown by the K_F values (magnitude 10^2 M^{-1}) which are in tandem with medium interactions. The number of binding sites (n) for both complexes **4** and **5** are approximately equal to one, indicating that there is a single binding site on the DNA molecule for the Re(I) complexes. Generally, there is a strong correlation observed between the binding strength values calculated from the UV–Vis titration experiments and those from the fluorescence measurements.

2.7. *Protein interaction studies*

Serum albumin is an essential plasma protein responsible for the transportation of small molecules, including vitamins, hormones and drugs within the bloodstream. Moreover, it plays a crucial role in maintaining fluid balance within the circulatory system [127]. In this study bovine serum albumin (BSA) was used as a relevant model as it is

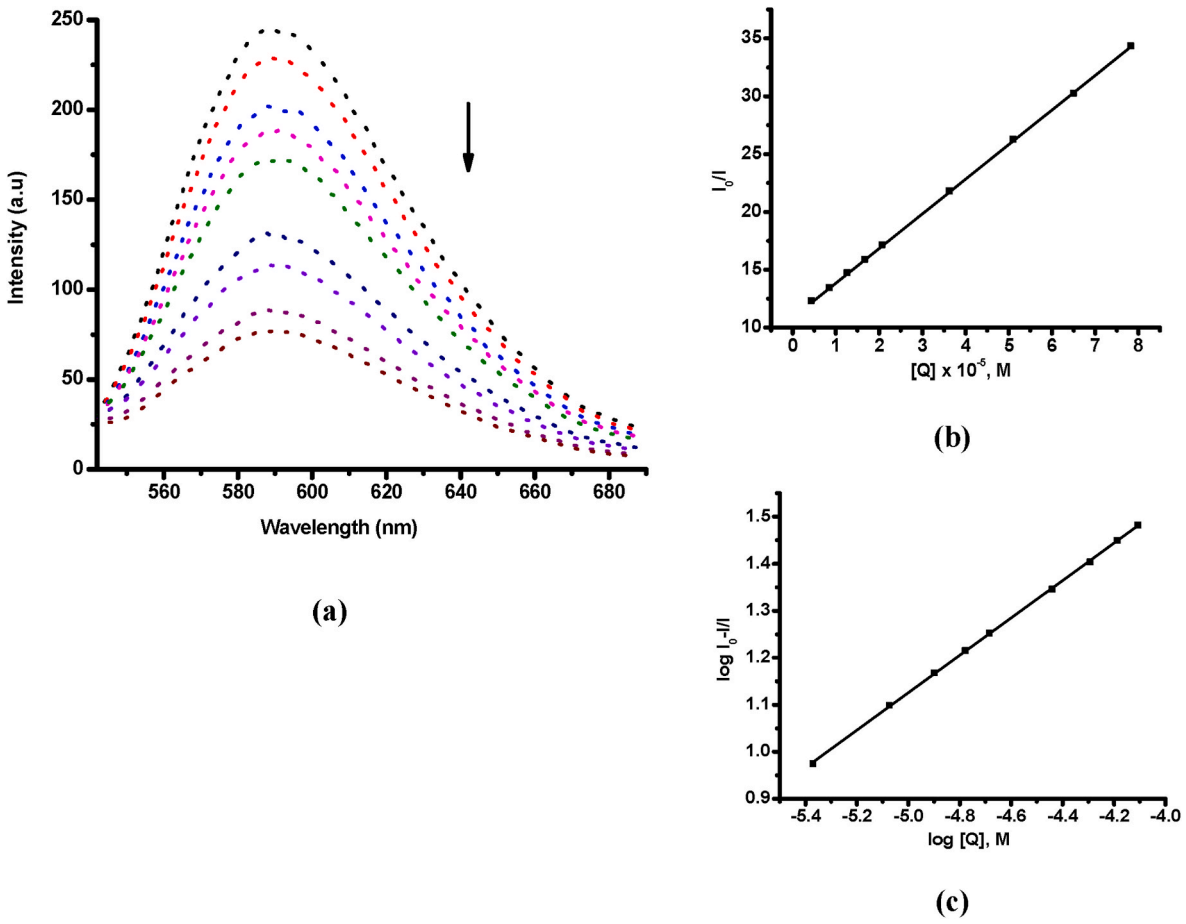

Fig. 9. (a) The effects of the addition of **4** on the emission intensity of EtBr bound to CT-DNA in the presence of varying amounts of **4** in PBS buffer (at pH = 7.2, 25 °C). [EtBr] = 20.0 μM, [CT-DNA] = 20.0 μM, and [**4**] = 0–150 μM. The arrow indicates the changes upon the addition of the metal complex. **(b)** Stern-Volmer plot of I_o/I vs. [*Q*]. **(c)** Scatchard plot of log[(I_o–*I*)/*I*] vs. log[*Q*].

structurally homologous to human serum albumin. BSA possesses an intrinsic fluorescence due to unique properties of the tyrosine, tryptophan and phenylalanine residues contained within the protein [128]. Fluorescence quenching has been widely used to evaluate the interaction of complexes with various proteins. Reduction in the fluorescence intensity of the fluorophore, specifically the tryptophan residue of BSA, is brought about by strong interactions between the complexes of interest and the protein [129,130]. The fluorescence spectra of BSA, maintained at a constant concentration of 1.5 μM in the presence of increasing amounts (0–30 μM) of the rhenium(I) complexes (**4, 5**) are depicted in Figs. 11 and 12. The spectra show a significant decrease in the fluorescence intensity of BSA as the concentration of the Re(I) complex increases, with no changes in the position of the emission wavelengths and shape of the peaks. As a result, complexes **4** and **5** demonstrate a remarkable ability to bind to BSA, inducing considerable conformational changes in its secondary structure while effectively quenching its intrinsic fluorescence [131]. This observation reveals a definite interaction occurring between both of the rhenium(I) complexes and BSA.

The changes in fluorescence intensities fit well with the Stern-Volmer (K_{sv} and k_q) and Scatchard (K_F and n) equations, and their corresponding values are shown in Table 4. The values of K_{SV} of magnitude 10^5 M^{-1} (Table 4), signify that the process of interaction between the complexes and the BSA protein is not fully controlled by diffusion, resulting in larger k_q values. The magnitude of the k_q values of **4** and **5** (10^{13} $M^{-1}s^{-1}$) exceed the maximum scattering collision rate observed in most known quenchers (2.0×10^{10} $M^{-1}s^{-1}$), suggesting the existence of a static quenching mechanism [132]. The values of K_{SV} and k_q for complexes **4** and **5** are similar to those reported for a series of Re(I) complexes [110, 133,134].

The K_F values of complexes **4** and **5**, which are of the order of 10^2 M^{-1}, are lower than the value of the association constant ($K_F = 10^{15}$ M^{-1}) of protein-ligand adducts with the highest binding capability [135]. In addition, the K_F magnitude strongly suggests that the interactions of **4** and **5** with BSA amino acids are predominantly due to hydrophobic interactions, specifically within subdomain IIA of the protein. Consequently, complexes **4** and **5** can easily be released from the protein upon reaching the target cells. Hence both complexes prove to be well-suited for facilitating drug-cell interactions. Furthermore, both **4** and **5** display *n* values that are close to unity, indicating the presence of a single binding on BSA.

2.8. Molecular docking

We employed molecular docking to gain an insight into the drug-receptor interactions. Complexes **4** and **5** were simulated in the DNA dodecamer with a sequence of d(CGCGAATTCGCG)$_2$ (PDB ID: 1BNA) binding pockets as shown in Fig. 13. The intermolecular interactions and binding affinities of the complexes within specific distances are given in Table 5. The docked poses of **4** and **5** depict intercalative modes of binding, consistent with the experimental results. Moreover, the binding scores of −6.6 kcal/mol (**4**) and −6.9 kcal (**5**) show a positive correlation with the experimentally determined binding constant values in Tables 2 and 3. Complex **4** forms carbon hydrogen bond and conventional hydrogen bond interactions with nucleotides DC23 (3.39 Å) and DG22 (2.33 Å), respectively. As for complex **5**, it interacts with DC3

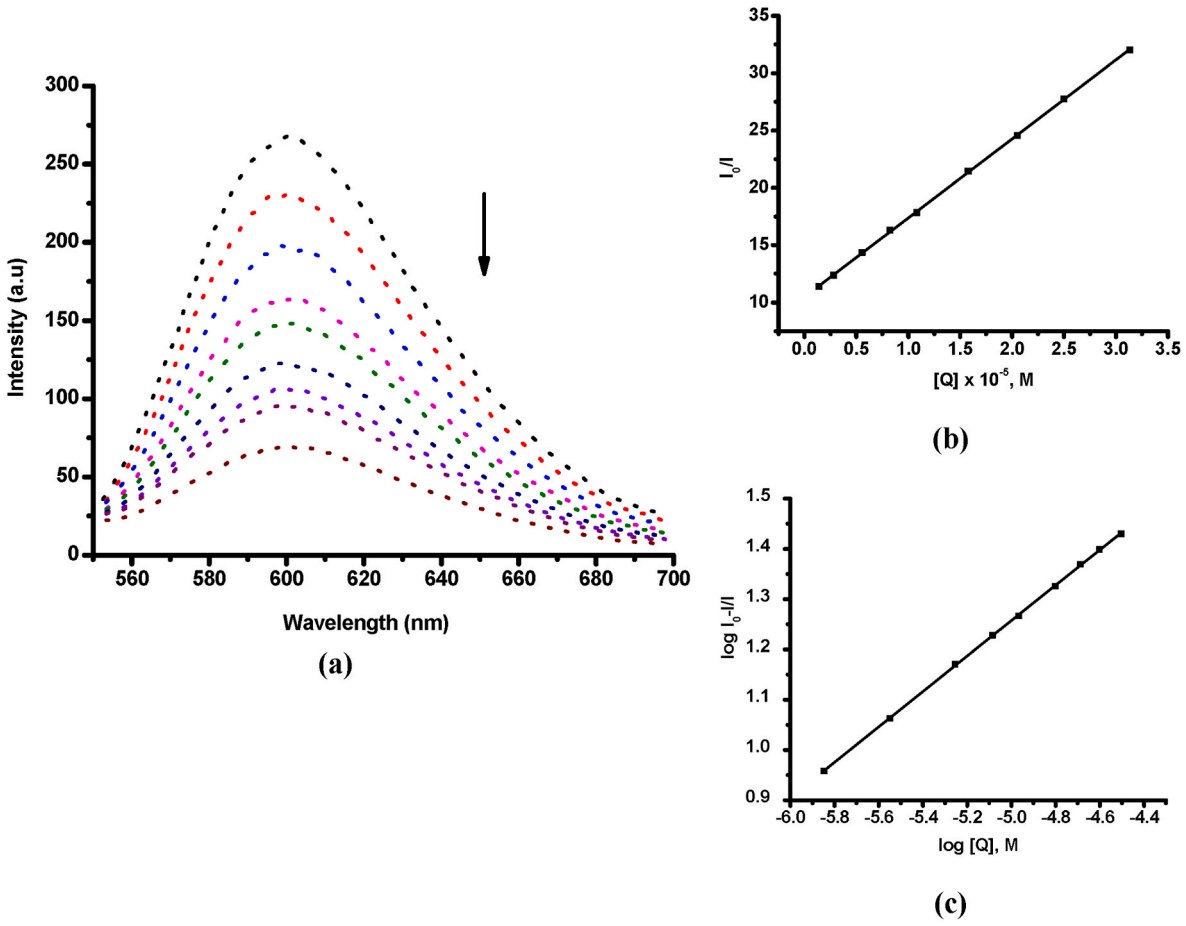

Fig. 10. (a) The effects of the addition of **5** on the emission intensity of EtBr bound to CT-DNA in the presence of varying amounts of **5** in PBS buffer (at pH = 7.2, 25 °C). [EtBr] = 20.0 μM, [CT-DNA] = 20.0 μM, and [**5**] = 0–150 μM. The arrow indicates the changes upon the addition of the metal complex. **(b)** Stern-Volmer plot of I_o/I vs. [Q]. **(c)** Scatchard plot of log[$(I_o–I)/I$] vs. log[Q].

Table 3
Fluorescence quenching parameters for the interactions of complexes **4** and **5** with CT-DNA.

Compound	K_{SV} (10^5 M^{-1})	k_q (10^{13} M^{-1} s^{-1})	K_{app} (10^6 M^{-1})	K_F (10^2 M^{-1})	n
4	2.88 ± 0.38	1.30 ± 0.25	5.51 ± 0.42	1.19 ± 0.10	0.96
5	7.91 ± 0.67	3.04 ± 0.31	14.06 ± 0.90	2.12 ± 0.14	1.01

(2.62 Å) and DG4 (2.03 Å) via conventional hydrogen bond interactions. In addition, the stability of **5** is considerably contributed by an attractive charge interaction with DG24 (5.38 Å).

The interactions of **4** and **5** with the BSA protein are illustrated in Fig. S18. Binding energies and a list of intermolecular interactions with the active amino acids are provided in Table S4. Notably, hydrophobic interactions were observed between complexes **4** and **5** and amino acids residues. The most stable pose of **4** depicts interactions with: ALA349, 4.92 Å and VAL215, 4.53 Å (alkyl interactions); LEU330, 4.89 Å and ARG208 5.49 Å (pi-alkyl interactions); GLU353, 2.91 Å and VAL481, 2.19 Å (conventional hydrogen bond interactions); PHE205, 5.44 Å (pi-pi T-shaped interactions) and LYS211, 4.81 Å (amide-pi stacked interactions). Similarly, complex **5** establishes pi-alkyl interactions (with LYS114, 5.14 Å; ARG144, 4.35 Å; LEU112, 5.09 Å; ARG196,3.71 Å; ALA193, 4.46 Å; LEU189, 4.10 Å), conventional hydrogen bond interactions (with ASP108, 2.70 Å; ARG458, 2.96 Å; ASP111, 2.94 Å) and pi-pi-T-shaped interactions (with HIS145, 4.86 Å). The docked energies of both complexes are relatively the same (−8.0 ± 0.1 kcal/mol), with highly favourable best-docked conformations.

3. Conclusions

A pair of 4-aminoquinoline Schiff base ligands (**2, 3**) containing an iminoquinolyl or iminopyridyl entity were successfully synthesized and coordinated to the Re(I) tricarbonyl core *via N,N*-chelation, producing the corresponding metal complexes (**4, 5**) in good yields. The synthesized ligands (**2, 3**) and complexes (**4, 5**) were fully characterized using various spectroscopic and analytical techniques. Single crystals of the pyridyl-substituted ligand (**2**) and the corresponding Re(I) complex (**4**) were analysed by X-ray diffraction, confirming numerous structural characteristics that were corroborated by spectroscopic measurements. Results from the cytotoxicity assays suggest that metal complexation, with the $[Re(CO)_3Cl]^+$ core (**4, 5**), significantly enhanced the activity of the corresponding, uncoordinated ligands (**2, 3**). Both Re(I) complexes (**4, 5**) showed superior cytotoxic activity compared to cisplatin against both the hormone-dependent (MCF-7) and hormone-independent (MDA-MB-231) breast cancer cell lines, with the iminoquinolyl-coordinated complex **5** being up to 3.6 times more potent than the clinical drug. The Re(I) complexes (**4, 5**) displayed moderate activity against the highly aggressive and invasive MDA-MB-231 cell line; however, they were far more potent against the hormone-dependent MCF-7 cell line. Overall, the iminoquinolyl-coordinated complex **5** was more potent, relative to the iminopyridyl-coordinated analogue **4**, towards the tested breast cancer cell lines. Of significance, the more

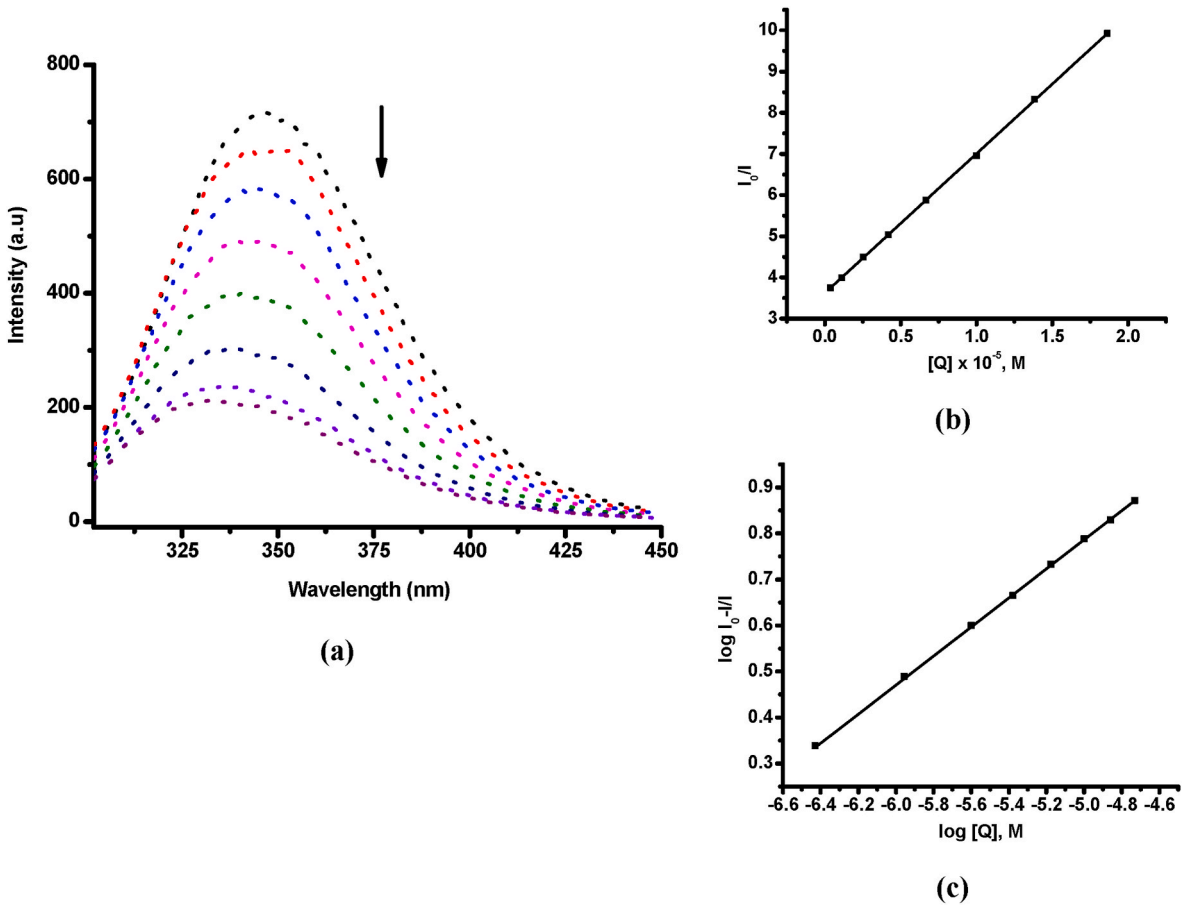

Fig. 11. (a) Fluorescence emission spectra of BSA protein in the absence and presence of complex **4**. BSA [1.5 μM] in the presence of consecutive quantities of **4** [0–30 μM]. The arrow shows the intensity changes upon increasing the concentration of **4**. (b) Stern–Volmer plot of I_o/I vs. [*Q*]. (c) Scatchard plot of log[(I_o–*I*)/*I*] vs. log[*Q*].

cytotoxic complex **5** was also the more selective complex with an S.I. value over 1, showing selectivity towards the MCF-7 breast cancer cell line over the FG-0 non-tumorigenic cell line. Due to rhenium-based complexes being relatively underexplored in terms of their promising anticancer activity, further investigations are warranted to understand their mechanism of actions. In that regard, western blot experiments revealed that complexes **4** and **5** triggered the upregulation of principal molecular markers for DNA damage and apoptosis. Absorption spectral studies established that the interactions between the complexes and DNA to be of an intercalative nature; these observations were further supported by competitive binding studies with ethidium bromide. In addition, protein interaction studies monitored by fluorescence emission spectroscopy showed favourable interactions between BSA and both Re (I) complexes. The DNA and protein binding results were confirmed through *in silico* molecular docking simulations where the complexes exhibited strong intermolecular interactions with double-stranded DNA and similarly with the amino acid residues of BSA. It is noteworthy that the quinolyl-substituted complex **5** exhibits greater binding affinity to DNA and the highest cytotoxic activity against the tested breast cancer cell lines. These observations suggest that a superior interaction with DNA may be associated with an enhanced activity against the cancer cell lines. Further, the additional quinoline scaffold appears to contribute significantly to the cytotoxic activity and biomolecule interactions displayed by the complex, thus emphasizing the invaluable pharmaco-properties of the quinoline structure.

4. Experimental

4.1. General methods and chemicals

All reagents and solvents were commercially sourced (Sigma-Aldrich, Merck and Kimix) and used without further purification. Compounds **1** and **2** were synthesized following literature methods [63, 64]. All solvents used were reagent grade and dried over molecular sieves, where required. All aqueous solutions (NaOH, NaCl, $NaHCO_3$) were prepared using deionized water. Synthetic procedures were carried out under nitrogen atmosphere using standard Schlenk line techniques unless otherwise stated. Reactions were monitored by thin-layer chromatography (TLC) using aluminium-backed precoated silica gel 60 F254 or neutral alumina oxide 60 F254 plates and viewed under ultraviolet (UV) light at 254 nm.

4.2. Spectroscopic and analytical techniques

Nuclear magnetic resonance (NMR) spectra were obtained using a Bruker XR600 MHz spectrometer (^{1}H at 599.95 MHz and ^{13}C{^{1}H} at 151.0 MHz), a Bruker XR400 spectrometer (^{1}H at 399.95 MHz and ^{13}C{^{1}H} at 100.58 MHz) or a Varian Mercury 300 (^{1}H at 300.08 MHz) spectrometer. Chemical shifts are recorded in ppm (δ) and *J*-coupling values reported in Hz with tetramethylsilane (TMS) used as the internal standard. The signals were assigned as follows: s, singlet; d, doublet; dd, doublet of doublets; dt, doublet of triplets; t, triplet; m, multiplet; br.s, broad singlet. Fourier-transform infrared (FT-IR) spectroscopy was performed on a Perkin-Elmer Spectrum 100 FT-IR spectrometer using a

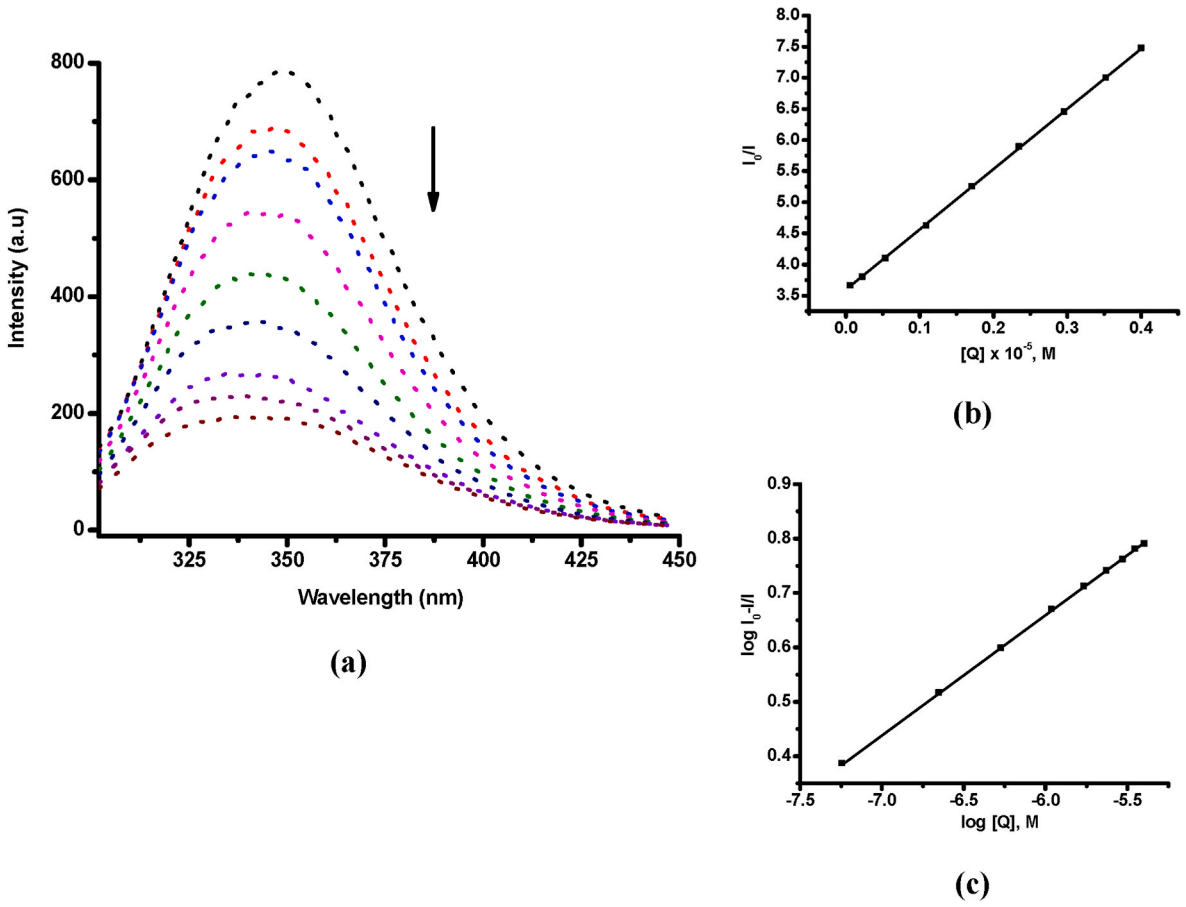

Fig. 12. (a) Fluorescence emission spectra of BSA protein in the absence and presence of complex **5**. BSA [1.5 μM] in the presence of consecutive quantities of **5** [0–30 μM]. The arrow shows the intensity changes upon increasing the concentration of **5**. (b) Stern–Volmer plot of I_o/I vs. [Q]. (c) Scatchard plot of log[(I_o–I)/I] vs. log[Q].

Table 4
Fluorescence quenching parameters for the interaction between complexes **4** and **5** and BSA protein.

Compound	K_{SV} (10^5 M^{-1})	k_q (10^{13} M^{-1} s^{-1})	K_F (10^2 M^{-1})	n
4	3.37 ± 0.19	1.47 ± 0.25	1.93 ± 0.12	0.99
5	9.79 ± 0.44	4.19 ± 0.32	2.58 ± 0.11	1.13

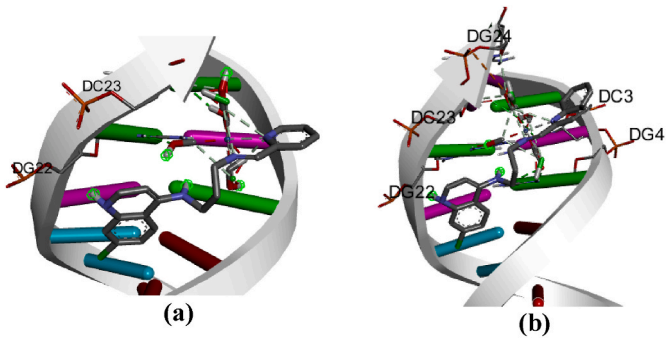

Fig. 13. The best docked conformer of (a) complex **4** and (b) complex **5** with DNA duplex depicting intercalative binding.

KBr pellet and fitted with an Attenuated Total Reflectance (ATR) unit. The measurements of bond vibrations were recorded in reciprocal centimetres (cm^{-1}).

Table 5
Interaction properties of complexes **4** and **5** analysed by Discovery Studio Visualizer.

Compound	Docking score (kcal/mol)	Carbon H-bond (Å)	Conventional H-bond (Å)	Attractive charge (Å)
4	−6.6	DC23 (3.39 Å)	DG22 (2.33)	–
5	−6.9	–	DC3 (2.62) DG4 (2.03)	DG24 (5.38)

The more negative the free binding energy, the stronger the binding affinity. Numbers indicated within brackets represent the distance of interacting atoms in Angstrom (Å).

Electronic absorption (UV–Vis) spectra were recorded using an Agilent Cary 8454 UV–Vis spectrometer, recording in the range of 250 nm and 800 nm. Fluorescence emission spectra were recorded using a Perkin Elmer LS 45 Fluorescence Spectrometer using 1 cm path length cuvettes at room temperature. Melting points were measured using a Büchi Melting Point Apparatus B-540 and are uncorrected. High resolution (HR) electrospray ionisation mass spectrometry (ESI-MS) was performed, using the positive ion-mode, on a Waters Synapt G2 mass spectrometer equipped with an ESI probe. The Agilent HPLC 1260 equipped with an Agilent DAD 1260 UV–Vis detector and an Agilent Pursuit 5C18 column (5 μM pore size, 150 mm × 4.6 mm) was utilized to evaluate the purity of the complexes prepared and used in this study. The compounds were eluted using a mixture of solvent A (H_2O) and solvent B (MeOH) at a flow rate of 1.0 mL min^{-1}, with the detection

wavelength set at 254 nm. The gradient elution conditions were as follows: 30% solvent A between 0 and 1 min, 30–90% solvent from 1 to 10 min, 90 to 10% solvent A from 10 to 20 min.

4.3. Synthesis

4.3.1. 7-Chloro-N-(3-((quinolin-2-ylmethylene)amino)propyl)quinolin-4-amine (3)

Precursor compound **1** (0.291 g, 1.23 mmol) and 2-quinoline carboxaldehyde (0.221 g, 1.41 mmol) were dissolved in anhydrous methanol (20.0 mL). Dry 3 Å molecular sieves were then added to the reaction flask. This was allowed to stir at 30 °C for 48 h. The reaction mixture was then cooled to room temperature and the molecular sieves were removed via filtration and washed with excess methanol. The solvent was removed under reduced pressure, the resulting residue was re-dissolved in dichloromethane (50.0 mL) and subsequently washed with water (3 × 20.0 mL). The organic layers were collected and dried over anhydrous $MgSO_4$, filtered and the solvent was then removed *in vacuo*. Purification was performed via recrystallisation by dissolving the crude in minimal CH_2Cl_2 followed by inducing precipitation by layering the solution with diethyl ether. Compound **3** was isolated as a light-yellow solid. Yield: 0.323 g (70%). ^{1}H NMR (300 MHz, CD_2Cl_2) δ (ppm) = 8.59 (1H, s, H_n), 8.48 (1H, d, J = 5.3 Hz, H_b), 8.28 (1H, d, J = 8.6 Hz, H_g), 8.17 (1H, d, J = 8.5 Hz, H_p), 8.10 (1H, d, J = 8.4 Hz, H_q), 7.97–7.85 (2H, m, $H_{u,v}$) 7.77 (2H, m, $H_{d,s}$), 7.62 (1H, t, J = 7.5 Hz, H_t) 7.23 (1H, d, J = 8.9 Hz, H_f), 6.45 (1H, d, J = 5.3 Hz, H_a), 6.12 (1H, s, H_j), 3.95 (2H, t, J = 5.9 Hz, H_m), 3.53 (2H, q, J = 5.9 Hz, H_k), 2.29–2.16 (2H, m, H_l), 1.98 (1H, s, *N*-H_j···N═C). ^{13}C{^{1}H} NMR (101 MHz, CD_2Cl_2): δ (ppm) = 163.91, 154.90, 152,50, 150,29, 149.65, 148.32, 136.93, 134.77, 130.31, 130.02, 129.17, 129.00, 128.19, 128.00, 125.09, 122.05, 118.54, 117.75, 99.30, 60.62, 43.24, 29.93. IR (ATR): (ν_{max}/cm^{-1}) 3238 (*sec.* NH), 1576 (C═N)$_{imine,\ quinolyl}$, 1558 (C═N)$_{quinoline}$. UV–Vis (DMSO): λ_{max} nm (10^{-4} ε, mol^{-1} L cm^{-1}) 334 (0.601). Melting point: 168.5–169.4 °C. MS (HR-ESI, *m/z*): 397.0992 (70%, $[M + Na]^+$), calculated 397.1196.

4.3.2. Re(I) aminoquinoline-pyridyl complex (4)

A solution of compound **2** (0.0688 g, 0.212 mmol) and $[Re(CO)_5Cl]$ (0.0813 g, 0.225 mmol) was prepared in anhydrous methanol (20.0 mL), and refluxed at 65 °C for 18 h. The reaction flask was covered in foil for the duration of the reaction. After completion of the reaction, the mixture was cooled to room temperature and the solvent was reduced to dryness by rotary evaporation. The crude compound was re-dissolved in a minimal volume of CH_2Cl_2 and then precipitated with diethyl ether. The orange precipitate was isolated by filtering under vacuum followed by washing it with diethyl ether. Recrystallisation of the isolated orange powder in minimal CH_2Cl_2 followed by slow diffusion of diethyl ether produced the pure compound (**4**) as orange needles. Yield: 0.0903 g (68%). ^{1}H NMR (600 MHz, $(CD_3)_2(CO)$): δ (ppm) = 9.33 (1H, s, H_n), 9.10 (1H, d, J = 5.3 Hz, H_s) 8.45 (1H, d, J = 5.5 Hz, H_b), 8.29 (2H, td, J = 7.8, 1.4 Hz, H_q), 8.24 (1H, d, J = 9.0 Hz, H_g), 8.17 (1H, d, J = 7.7 Hz, H_p), 7.87 (1H, d, J = 2.1 Hz, H_d), 7.83 (1H, m, H_r), 7.33 (1H, dd, J = 9.0, 2.2 Hz, H_f), 7.16 (1H, s, H_j), 6.6 (1H, d, J = 5.6 Hz, H_a), 4.42 (2H, t, J = 6.5 Hz, H_m), 3.72–3.56 (2H, m, H_k), 2.64 (1H, m, H_l), 2.48 (1H, m, H_l). ^{13}C{^{1}H} NMR (151 MHz, $(CD_3)_2(CO)$): δ (ppm) = 198.77, 198.47, 188.43, 170.64, 156.36, 154.01, 151.82, 141.08, 135.47, 130.01, 129.82, 128.05, 125.58, 124.65, 118.55, 100.08, 66.23, 64.09, 41.51, 28.86, 15.68. IR (ATR): (ν_{max}/cm^{-1}) 3214 (*sec.* NH), 2014 (C═O), 1862 (C═O), 1573 (C═N)$_{imine,\ pyridyl}$, 1549 (C═N)$_{quinoline}$. UV–Vis (DMSO): λ_{max} nm (10^{-4} ε, mol^{-1} L cm^{-1}) 336 (0.890), 385 sh (0.378). Melting point: 213.8–214.9 °C. MS (HR-ESI, *m/z*): 631.0297 (100%, $[M + H]^+$), calculated 631.0235. HPLC purity: 98% ($t_{r'}$ = 2.36 min).

4.3.3. Re(I) aminoquinoline-quinolyl complex (5)

Ligand **3** (0.104 g, 0.276 mmol) was dissolved in anhydrous methanol (20.0 mL), after which $[Re(CO)_5Cl]$ (0.101 g, 0.280 mmol) was added. The reaction was refluxed at 65 °C overnight. The reaction flask was covered in foil for the duration of the reaction. After completion of the reaction, the mixture was cooled to room temperature and the solvent was reduced to dryness by rotary evaporation. The crude compound was re-dissolved in minimal CH_2Cl_2 and then precipitated with diethyl ether to yield an orange solid (**5**). Yield: 0.111 g (59%). ^{1}H NMR (600 MHz, CD_2Cl_2): δ (ppm) = 8.92 (1H, s, H_n), 8.84 (1H, d, J = 8.9 Hz, H_v), 8.46 (1H, d, J = 5.5 Hz, H_b), 8.36 (1H, d, J = 8.2 Hz, H_q), 8.09–8.04 (1H, m, H_u), 8.01 (1H, d, J = 8.2 Hz, H_s), 7.86 (1H, m, H_t), 7.83 (1H, d, J = 2.0 Hz, H_d), 7.71 (1H, d, J = 8.9 Hz, H_g), 7.44 (1H, d, J = 8.2 Hz, H_p),6.70 (1H, dd, J = 8.9, 2.1 Hz, H_f), 6.46 (1H, d, J = 5.5 Hz, H_a), 6.08 (1H, s, H_j), 4.58 (1H, m, H_m), 4.39 (1H, m, H_m), 3.62 (2H, m, H_k), 2.91–2.81 (1H, m, H_l), 2.52–2.42 (1H, m, H_l). ^{13}C{^{1}H} NMR (151 MHz, CD_2Cl_2): δ (ppm) = 197.93, 196.34, 186.99, 170.30, 156.36, 151.56, 150.53, 148.16, 141.11, 135.18, 133.88, 130.56, 130.35, 130.06, 129.41, 128.01, 125.24, 123.28, 123.04, 117.46, 99.23, 65.91, 42.72, 27.85. IR (ATR): (ν_{max}/cm^{-1}) 3224 (*sec.* NH), 2011 (C═O), 1910 (C═O), 1863 (C═O), 1574 (C═N)$_{imine,\ quinolyl}$, 1524 (C═N)$_{quinoline}$. UV–Vis (DMSO): λ_{max} nm (10^{-4} ε, mol^{-1} L cm^{-1}) 333 (1.39), 420 (0.330). Melting point: >170.2 °C dec. without melt. MS (HR-ESI, *m/z*): 679.0280 (100%, $[M - H]^-$), calculated 679.0392; 681.0483 (80%, $[M + H]^+$), calculated 681.0552. HPLC purity: 99% ($t_{r'}$ = 2.05 min).

4.4. Single crystal X-ray crystallography

Suitable single crystals of ligand **2** and complex **4** were grown from the layering of diethyl ether into a concentrated dichloromethane solution, followed by slow evaporation of solvent at room temperature. A Bruker D8 Venture diffractometer with graphite-monochromated Cu-Kα radiation (λ = 1.54178 Å) was utilized to obtain single-crystal X-ray diffraction data of the prepared crystals. The data was collected at a temperature of 100(2) K and controlled by an Oxford Cryostream cooling system (Oxford Cryostat). The program SAINT was used to conduct cell refinement and data reduction [136]. The data were scaled, and absorption correction carried out using SADABS [137]. The structures were solved using SHELXS-97 [137] by means of direct methods, refined via full-matrix least-squares methods based on F^2 by operating both SHELXL-2014 [137] and the graphics interface program, X-Seed [138,139]. The X-Seed and POV-Ray [138,140] programs were utilized to produce graphical images of the molecular structures. All non-hydrogen atoms contained within the structures were refined anisotropically. Additionally, all hydrogen atoms, except the amino hydrogen H2, were arranged in idealised positions and refined in riding models where, U_{iso} was assigned 1.2 or 1.5 times U_{eq} of the parent hydrogen atoms. Further, the C–H bond distances were constrained to the range between 0.95 Å to 0.99 Å. The hydroxyl hydrogens and the hydrogens on N2, of ligand **2**, were located in the difference density maps and refined independently. The structure of ligand **2** was refined to R factor of 0.0433. In addition, the hydrogen H2 on N2, of complex **4**, was found in the difference density maps and refined independently. The structure of complex **4** was refined to R factor of 0.0215.

4.5. Solution stability studies

The stability of complexes **4** and **5** was carefully observed in a solution of PBS supplemented with 1% DMSO over a 48-hour period at 37°C, employing UV-Vis spectroscopy.

4.6. Biological studies

4.6.1. Cell culture

Roswell Park Memorial Institute (RPMI) 1640 medium (Sigma-Aldrich, USA) was used to maintain the human breast adenocarcinoma cell line, MCF-7, which is oestrogen-receptor positive (ER+). While the human breast adenocarcinoma cell line, MDA-MB-231, a triple negative

breast cancer (TNBC), and the non-malignant dermal fibroblast cells, FG-0, were maintained in Dulbecco's Modified Eagle's Medium (DMEM) (Sigma-Aldrich, USA). The culture media were supplemented with 10% heat-inactivated foetal bovine serum (FBS), 100 U/mL of penicillin and 100 μg/mL streptomycin. To maintain physiological pH and temperature, all cells were nurtured in a 95% air and 5% CO_2 humidified incubator and maintained at 37 °C. Additionally, the culture media were replenished with fresh media every 48–72 h.

4.6.2. Cytotoxicity assays

The MCF-7, MDA-MB-231 and FG-0 cells were seeded on a 96-well plate at densities of 4500 cells/well, 3000 cells/well and 1500 cells/well, respectively. Under physiological conditions, the MCF-7 and FG-0 cells were incubated for 48 h and the MDA-MB-231 cells for 24 h, to allow for adhesion. Once adhered the MCF-7 and MDA-MB-231 cells were treated with either the vehicle (0.1% DMSO in growth media) or the test compounds at 10 μM or 20 μM and incubated for 48 h. The 3-(4,5-dimethylthiazol-2-yl)-2,5-diphenyltetrazolium bromide (MTT) assay was used to determine the effect of the test compounds on the cancer cell viability, as described in literature [93]. The MTT colorimetric assay is based on the NAD(P)H-dependent oxidoreductase enzymes produced by actively growing cells. These cells catalyse the reduction of MTT to purple formazan crystals [141]. The absorbance of each well was measured at 600 nm using a spectrophotometer (GloMax® Explorer Multimode Microplate Reader GM3500, Promega) and normalized to the RPMI medium (for the MCF-7 cell line) or the DMEM growth media (for the MDA-MB-231 and FG-0 cell lines) [142]. The MCF-7, MDA-MB-231 and FG-0 cell lines were treated with concentrations ranging from 0 to 35 μM of the tested complexes to determine their IC_{50} (concentration required for 50% viability). All experiments were performed twice in triplicate, and the mean cell viability determined using the GraphPad Prism V.5.01 software.

4.6.3. Western blotting

MCF-7 and MDA-MB-231 cells were seeded in 6 cm dishes and treated for 48 h with complexes **4** and **5** at the ½ IC_{50} and IC_{50} concentrations. The relevant proteins were extracted and prepared from the treated cells, thereafter, subjected to SDS-PAGE and immunoblotting following the procedure formerly described by Bleloch et al. [143] The primary antibodies utilized in this study, rabbit polyclonal antibodies to Phospho-Histone γH2A.X (Ser139) (#2577), PARP (#9542) and mouse monoclonal anti-β-Actin (sc-47778), were supplied by Cell Signaling Technology (USA). The secondary antibodies were used at a dilution of 1:5000 and comprised of horseradish peroxidase–conjugated goat anti-rabbit (Bio-Rad) and goat anti-mouse (Bio-Rad). Densitometry was executed with the image analysis software Fiji (Version 2.0.0-rc-68/1.52e). The levels of protein expression were represented as a ratio of the protein of interest/β-actin loading control and normalized to the control sample, where appropriate. All blots are indicative of no less than three independent repeats.

4.7. DNA interaction studies

4.7.1. Absorption spectroscopic studies

All experiments regarding DNA interactions with complexes **4** and **5** were carried out in PBS buffer with pH = 7.2, at ambient temperature. The concentration of CT-DNA solution in PBS buffer was determined spectrophotometrically with a molar extinction coefficient $\varepsilon_{260} = 6600$ mol^{-1} cm^{-1}. The purity of the CT-DNA solution in PBS buffer was confirmed from the ratio of electronic absorption at 260 nm. Standard stock solutions of the rhenium complexes (**4**–**5**) were prepared with 5% DMSO and 95% ultrapure water.

Absorption spectra of CT-DNA maintained at constant concentrations of 50 μM, were recorded with increasing amounts of metal-complexes (0–350 μM). The solutions were incubated for 8 min at ambient temperature prior to recording the absorption spectra at a range of 250–400 nm. The intrinsic binding constant, K_b, for each complex is estimated using Eq. (1) 101.

$$1/A - A_0 = 1/K_b.\ \Delta\varepsilon.\ 1/[complex] + 1/A_0 \quad (1)$$

where A is the recorded absorption at different metal concentrations; A_0 is the initial absorption of CT-DNA at 260 nm; $\Delta\varepsilon$ is the molar absorptivity change upon complex formation; [complex] is the concentration of the metal complex.

The standard Gibb's free energy (ΔG) for each experiment was calculated following the van't Hoff Eq. (2) [112].

$$\Delta G = -RT \ln K_b. \quad (2)$$

4.7.2. Ethidium bromide (EtBr) displacement studies

The CT-DNA-EtBr (calf thymus DNA – ethidium bromide) composite was prepared at a molar ratio of 1:1 EtBr:CT-DNA (10 μM each) in PBS buffer solution (pH = 7.2, 25 °C) and kept in the dark for the experiment. The concentration of the CT-DNA-EtBr composite was kept constant while the quencher (the Re(I) complex) was added in increments of 0–150 μM, at ambient temperature. The fluorescence emission was excited at 525 nm, and the emission recorded, at ambient temperature, at a range of 530 nm–700 nm, following a 10 min incubation period. The Stern-Volmer binding constant (K_{SV}), and the bimolecular quenching rate constant (k_q) were computed from the classical Stern-Volmer Eq. (3) [118].

$$I_o/I = 1 + K_{sv}[Q] = 1 + k_q\tau_0[Q]w \quad (3)$$

here I_o and I are the emission intensities in the absence and presence of the Re(I) complex (quencher), respectively; [Q] is the concentration of the Re(I) complex, and τ_0 is the average lifetime of the fluorophore (10^{-8} s) without the Re(I) complex.

The apparent association constant, K_{app}, was obtained using Eq. (4) [125].

$$K_{EtBr}[EtBr] = K_{app}[Q] \quad (4)$$

where [Q] is the concentration of the Re(I) complex that causes a 50% reduction in the intensity of the CT-DNA-EtBr fluorescence, and $K_{EtBr} = 10^7$ M^{-1}. The binding constant, K_F, and the number of binding sites (n) were estimated from the Scatchard Eq. (5) [126].

$$\log(I_o - I)/I = \log K_F + n \log[Q] \quad (5)$$

4.8. Protein interaction studies

The studies were conducted in a similar manner as outlined above, for the CT-DNA-EtBr emissions. The concentration of PBS buffer was spectrophotometrically determined at a molar extinction coefficient of ε_{280} = 44,300 mol^{-1} cm^{-1}. The concentration of BSA protein was maintained at 1.5 μM, while the quencher, i.e. Re(I) complex, was added in increments from 0 μM to 30 μM, at ambient temperature. Following a 10 min period of incubation, at ambient temperature, the samples were excited at a wavelength of 280 nm and the emission spectra were recorded from 300 nm to 450 nm.

Following literature procedures [144], data corrections of the spectrophotometric titrations were employed, to account for the existing primary and/or secondary inner filter effects, by applying Eq. (6).

$$F_{corr} = F_{obs}10(A_{ex} + A_{em})/2w \quad (6)$$

here F_{corr} and F_{obs} are the corrected and observed fluorescence intensities, respectively; whilst A_{ex} and A_{em} are the absorbance values at the excitation and emission wavelengths, respectively.

4.9. Molecular docking

The crystal structures of DNA (PDB ID: 1Z3F) and BSA (PDB ID:4F5S) were obtained from the RCSB protein data bank (http://www.rcsb.org/) at a solution of 1.60 and 2.47 Å, respectively. The structures were refined by removing any co-crystallized hetero ligands, waters, and/or cofactors. Thereafter, polar hydrogen atoms and Kollman charges were added to the structures. Gasteiger charges were calculated and assigned to each atom accordingly, and non-polar hydrogen atoms were merged into carbon atoms. The coordination spheres of the metal complexes were generated from DFT calculations, and the GaussView 5.0 software was used to convert the complexes' optimized geometry and lowest energy conformations to the appropriate PDB format. The complexes and receptors (i.e. DNA and BSA) were prepared using AutoDock Tools. The molecular docking investigations were performed using the PyRx program [145]. During the docking analyses, the binding sites were constrained to the entire receptor, where a grid spacing of 0.375 Å was applied. The BIOVIA Discovery Studio Visualizer 2022 package was used to visualize the predicted interactions and prepare the structural graphics, molecular animations, and atomic interaction measurements. The predicted binding affinities were obtained in terms of binding energies in kcal/mol and assigned as their docking scores.

CRediT authorship contribution statement

Paige S. Zinman: Writing – original draft, Validation, Investigation, Formal analysis, Data curation. **Athi Welsh:** Investigation. **Reinner O. Omondi:** Writing – review & editing, Investigation. **Saif Khan:** Investigation. **Sharon Prince:** Supervision, Resources, Investigation. **Ebbe Nordlander:** Writing – review & editing. **Gregory S. Smith:** Writing – review & editing, Supervision, Resources, Project administration, Funding acquisition, Conceptualization.

Declaration of competing interest

The authors declare that they have no known competing financial interests or personal relationships that could have appeared to influence the work reported in this paper.

Data availability

Data will be made available on request.

Acknowledgements

We gratefully acknowledge and thank the University of Cape Town and the National Research Foundation of South Africa (UID: 129288) for financial support. Prof S. Prince gratefully acknowledges and thanks the University of Cape Town, the National Research Foundation of South Africa (UID: 120815), the International Centre for Genetic Engineering and Biotechnology (ICGEB) and the South African Medical Research Council (SAMRC) under a Self-Initiated Research Grant for financial support. The views and opinions expressed are those of the author(s) and do not necessarily represent the official views of the SAMRC.

Appendix A. Supplementary data

Supplementary data to this article can be found online at https://doi.org/10.1016/j.ejmech.2023.116094.

References

[1] A.G. Waks, E.P. Winer, Breast cancer treatment: a review, JAMA 321 (2019) 288.
[2] M. Arnold, E. Morgan, H. Rumgay, A. Mafra, D. Singh, M. Laversanne, J. Vignat, J.R. Gralow, F. Cardoso, S. Siesling, I. Soerjomataram, Current and future burden of breast cancer: global statistics for 2020 and 2040, Breast 66 (2022) 15.
[3] A.N. Giaquinto, H. Sung, K.D. Miller, J.L. Kramer, L.A. Newman, A. Minihan, A. Jemal, R.L. Siegel, Breast cancer statistics, 2022, CA, Cancer J. Clin. 72 (2022) 524.
[4] M. Vanneman, G. Dranoff, Combining immunotherapy and targeted therapies in cancer treatment, Nat. Rev. Cancer 12 (2012) 237.
[5] H. Schiff, Ann. Chem. Suppl. 3 (1864) 343.
[6] H. Schiff, Schiff base reaction, Justus Liebigs Ann. Chem. 131 (1864) 118.
[7] P. Sykes, A Guidebook to Mechanism in Organic Chemistry, sixth ed., Pearson Education Limited, Essex, England, 1986.
[8] S. Parveen, Recent advances in anticancer ruthenium Schiff base complexes, Appl. Organomet. Chem. 34 (2020) e5687.
[9] P.G. Cozzi, Metal–Salen Schiff base complexes in catalysis: practical aspects, Chem. Soc. Rev. 33 (2004) 410.
[10] T.P. Yoon, E.N. Jacobsen, Privileged chiral catalysts, Science 299 (2003) 1691.
[11] K. Brodowska, E. Lodyga-Chruscinska, Schiff bases - interesting range of applications in various fields of science, Chemik 68 (2014) 129.
[12] G. Moustafa, E. Sabry, E.M. Zayed, G.G. Mohamed, Structural characterization, spectroscopic studies, and molecular docking studies on metal complexes of new hexadentate cyclic peptide ligand, Appl. Organomet. Chem. 36 (2022) e6515.
[13] A. Singh, P. Barman, Recent advances in Schiff base ruthenium metal complexes: synthesis and applications, Top. Curr. Chem. 379 (2021) 29.
[14] D.N. Dhar, C. Taploo, Schiff-bases and their applications, J. Sci. Ind. Res. 41 (1982) 501.
[15] S. Shekhar, A.M. Khan, S. Sharma, B. Sharma, A. Sarkar, Schiff base metallodrugs in antimicrobial and anticancer chemotherapy applications: a comprehensive review, Emergent Mater 5 (2022) 279.
[16] K. Sztanke, A. Maziarka, A. Osinka, M. Sztanke, An insight into synthetic Schiff bases revealing antiproliferative activities in vitro, Bioorg. Med. Chem. 21 (2013) 3648.
[17] M.A. Malik, O.A. Dar, P. Gull, M.Y. Wani, A.A. Hashmi, Heterocyclic Schiff base transition metal complexes in antimicrobial and anticancer chemotherapy, MedChemComm 9 (2018) 409.
[18] G. Puthilibai, S. Vasudhevan, Synthesis, DNA binding, anticancer and cytotoxic evalutation of novel ruthenium(II) isatin based Schiff base complex, Rasayan J. Chem. 12 (2019) 855.
[19] A. Garza-Ortiz, P. Uma Maheswari, M. Siegler, A.L. Spek, J. Reedijk, A new family of Ru(ii) complexes with a tridentate pyridine Schiff-base ligand and bidentate co-ligands: synthesis, characterization, structure and in vitro cytotoxicity studies, New J. Chem. 37 (2013) 3450.
[20] G.A. Suárez-Ortiz, R. Hernández-Correa, M.D. Morales-Moreno, R.A. Toscano, M. T. Ramirez-Apan, A. Hernandez-Garcia, M. Amézquita-Valencia, D. Araiza-Olivera, Diastereomeric separation of chiral fac-Tricarbonyl(iminopyridine) rhenium(I) complexes and their cytotoxicity studies: approach toward an action mechanism against glioblastoma, J. Med. Chem. 65 (2022) 9281.
[21] A. Lapasam, V. Banothu, U. Addepally, M.R. Kollipara, Synthesis, structural and antimicrobial studies of half-sandwich ruthenium, rhodium and iridium complexes containing nitrogen donor Schiff-base ligands, J. Mol. Struct. 1191 (2019) 314.
[22] J. Shi, H. Ge, F. Song, S. Guo, Synthesis, characterization, crystal structure and antibacterial activity studies of cobalt(II) and zinc(II) complexes containing halogen quinoline Schiff base ligand, J. Mol. Struct. 1253 (2022) 132263.
[23] E. Yousif, A. Majeed, K. Al-Sammarrae, N. Salih, J. Salimon, B. Abdullah, Metal complexes of Schiff base: preparation, characterization and antibacterial activity, Arab. J. Chem. 10 (2017) S1639.
[24] R.K. Mohapatra, A.K. Sarangi, M. Azam, M.M. El-ajaily, M. Kudrat-E-Zahan, S. B. Patjoshi, D.C. Dash, Synthesis, structural investigations, DFT, molecular docking and antifungal studies of transition metal complexes with benzothiazole based Schiff base ligands, J. Mol. Struct. 1179 (2019) 65.
[25] E. Pahontu, F. Julea, T. Rosu, V. Purcarea, Y. Chumakov, P. Petrenco, A. Gulea, Antibacterial, antifungal and in vitro antileukaemia activity of metal complexes with thiosemicarbazones, J. Cell Mol. Med. 19 (2015) 865.
[26] M.S. More, P.G. Joshi, Y.K. Mishra, P.K. Khanna, Metal complexes driven from Schiff bases and semicarbazones for biomedical and allied applications: a review, Mater. Today Chem. 14 (2019) 100195.
[27] S. Shekhar, A.M. Khan, S. Sharma, B. Sharma, A. Sarkar, Schiff base metallodrugs in antimicrobial and anticancer chemotherapy applications: a comprehensive review, Emergent. Mater. 5 (2022) 279.
[28] A. Garza-Oritz, P. Uma Maheswari, M. Siegler, A.L. Spek, J. Reedijk, A new family of Ru(II) complexes with a tridentate pyridine Schiff-base ligand and bidentate co-ligands: synthesis, characterization, structure and in vitro cytotoxicity studies, New J. Chem. 37 (2013) 3450.
[29] E. Bulatov, R. Sayarova, R. Mingaleeva, R. Miftakhova, M. Gomzikova, Y. Ignatyev, A. Petukhov, P. Davidovich, A. Rizvanov, N.A. Barlev, Isatin-Schiff base-copper (II) complex induces cell death in p53-positive tumors, Cell Death Dis. 4 (2018) 103.
[30] M.J. Chow, M.V. Babak, D.Y.Q. Wong, G. Pastorin, C. Gaiddon, W.H. Ang, Structural determinants of p53-independence in anticancer ruthenium-arene Schiff-base complexes, Mol. Pharm. 13 (2016) 2543.
[31] V. Milosavljevic, Y. Haddad, M.A.M. Rodrigo, A. Moulick, H. Polanska, D. Hynek, Z. Heger, P. Kopel, V. Adam, The zinc-Schiff base-Novicidin complex as a potential prostate cancer therapy, PLoS One 11 (2016) e0163983.
[32] A. Lauria, G. La Monica, A. Bono, A. Martorana, Quinoline anticancer agents active on DNA and DNA-interacting proteins: from classical to emerging therapeutic targets, Eur. J. Med. Chem. 220 (2021) 113555.
[33] Y. Li, C. de Kock, P.J. Smith, H. Guzgay, D.T. Hendricks, K. Naran, V. Mizrahi, D. F. Warner, K. Chibale, G.S. Smith, Synthesis, characterization, and

pharmacological evaluation of silicon-containing aminoquinoline organometallic complexes as antiplasmodial, antitumor, and antimycobacterial agents, Organometallics 32 (2012) 141.
[34] T. Kimura, Y. Takabatake, A. Takahashi, Y. Isaka, Chloroquine in cancer therapy: a double-edged sword of autophagy, Cancer Res. 73 (2013) 3.
[35] E. Schrezenmeier, T. Dörner, Mechanisms of action of hydroxychloroquine and chloroquine: implications for rheumatology, Nat. Rev. Rheumatol. 16 (2020) 155.
[36] C. Verbaanderd, H. Maes, M.B. Schaaf, V.P. Sukhatme, P. Pantziarka, V. Sukhatme, P. Agostinis, G. Bouche, Repurposing drugs in oncology (ReDO)-chloroquine and hydroxychloroquine as anti-cancer agents, Ecancermedicalscience 11 (2017) 781.
[37] G. Manic, F. Obrist, G. Kroemer, I. Vitale, L. Galluzzi, Chloroquine and hydroxychloroquine for cancer therapy, Mol. Cell. Oncol. 1 (2014) e29911.
[38] W.A. Denny, Acridine derivatives as chemotherapeutic agents, Curr. Med. Chem. 9 (2002) 1655.
[39] B. Rosenberg, L. Vancamp, J.E. Trosko, V.H. Mansour, Platinum compounds: a new class of potent antitumour agents, Nature 222 (1969) 385.
[40] K.J. Franz, N. Metzler-Nolte, Introduction: metals in medicine, Chem. Rev. 119 (2019) 727.
[41] Z. Guo, P.J. Sadler, Metals in medicine, Angew. Chem. Int. Ed. 38 (1999) 1512.
[42] S. Monro, K.L. Colón, H. Yin, J. Roque, P. Konda, S. Gujar, R.P. Thummel, L. Lilge, C.G. Cameron, S.A. McFarland, Transition metal complexes and photodynamic therapy from a tumor-centered approach: challenges, opportunities, and highlights from the development of TLD1433, Chem. Rev. 119 (2019) 797.
[43] G. Gasser, N. Metzler-Nolte, The potential of organometallic complexes in medicinal chemistry, Curr. Opin. Chem. Biol. 16 (2012) 84.
[44] U. Ndagi, N. Mhlongo, M.E. Soliman, Metal complexes in cancer therapy - an update from drug design perspective, Drug Des. Dev. Ther. 11 (2017) 599.
[45] Q. Peña, A. Wang, O. Zaremba, Y. Shi, H.W. Scheeren, J.M. Metselaar, F. Kiessling, R.M. Pallares, S. Wuttke, T. Lammers, Metallodrugs in cancer nanomedicine, Chem. Soc. Rev. 51 (2022) 2544.
[46] C.C. Konkankit, S.C. Marker, K.M. Knopf, J.J. Wilson, Anticancer activity of complexes of the third row transition metals, rhenium, osmium, and iridium, Dalton Trans. 47 (2018) 9934.
[47] M. Galanski, M.A. Jakupec, B.K. Keppler, Update of the preclinical situation of anticancer platinum complexes: novel design strategies and innovative analytical approaches, Curr. Med. Chem. 12 (2005) 2075.
[48] C.-H. Leung, H.-J. Zhong, D.S.-H. Chan, D.-L. Ma, Bioactive iridium and rhodium complexes as therapeutic agents, Coord. Chem. Rev. 257 (2013) 1764.
[49] L. Galluzzi, L. Senovilla, I. Vitale, J. Michels, I. Martins, O. Kepp, M. Castedo, G. Kroemer, Molecular mechanisms of cisplatin resistance, Oncogene 31 (2012) 1869.
[50] K.M. Knopf, B.L. Murphy, S.N. MacMillan, J.M. Baskin, M.P. Barr, E. Boros, J. J. Wilson, In vitro anticancer activity and in vivo biodistribution of rhenium(I) tricarbonyl aqua complexes, J. Am. Chem. Soc. 139 (2017) 14302.
[51] I. Ott, R. Gust, Non platinum metal complexes as anti-cancer drugs, Arch. Pharm. 340 (2007) 117.
[52] A. Mondal, U. Sen, N. Roy, V. Muthukumar, S.K. Sahoo, B. Bose, P. Paira, DNA targeting half sandwich Ru(II)-p-cymene-N^N complexes as cancer cell imaging and terminating agents: influence of regioisomers in cytotoxicity, Dalton Trans. 50 (2021) 979.
[53] G. Gasser, I. Ott, N. Metzler-Nolte, Organometallic anticancer compounds, J. Med. Chem. 54 (2011) 3.
[54] A. Leonidova, G. Gasser, Underestimated potential of organometallic rhenium complexes as anticancer agents, ACS Chem. Biol. 9 (2014) 2180.
[55] A. Núñez-Montenegro, R. Carballo, E.M. Vázquez-López, Synthesis, characterization and binding affinities of rhenium (I) thiosemicarbazone complexes for the estrogen receptor (α/β), J. Inorg. Biochem. 140 (2014) 53.
[56] I. Kitanovic, S. Can, H. Alborzinia, A. Kitanovic, V. Pierroz, A. Leonidova, A. Pinto, B. Spingler, S. Ferrari, R. Molteni, A. Steffen, N. Metzler-Nolte, S. Wölfl, G. Gasser, A deadly organometallic luminescent probe: anticancer activity of a ReI bisquinoline complex, Chem. Eur J. 20 (2014) 2496.
[57] D. Giffard, E. Fischer-Fodor, C. Vlad, P. Achimas-Cadariu, G.S. Smith, Synthesis and antitumour evaluation of mono- and multinuclear [2+1] tricarbonylrhenium (I) complexes, Eur. J. Med. Chem. 157 (2018) 773.
[58] C.C. Konkankit, B.A. Vaughn, Z. Huang, E. Boros, J.J. Wilson, Systematically altering the lipophilicity of rhenium(i) tricarbonyl anticancer agents to tune the rate at which they induce cell death, Dalton Trans. 49 (2020) 16062.
[59] E.B. Bauer, A.A. Haase, R.M. Reich, D.C. Crans, F.E. Kühn, Organometallic and coordination rhenium compounds and their potential in cancer therapy, Coord. Chem. Rev. 393 (2019) 79.
[60] V.L. Gantsho, M. Dotou, M. Jakubaszek, B. Goud, G. Gasser, H.G. Visser, M. Schutte-Smith, Synthesis, characterization, kinetic investigation and biological evaluation of Re(i) di- and tricarbonyl complexes with tertiary phosphine ligands, Dalton Trans. 49 (2020) 35.
[61] P.T. Wilder, D.J. Weber, A. Winstead, S. Parnell, T.V. Hinton, M. Stevenson, D. Giri, S. Azemati, P. Olczak, B.V. Powell, T. Odebode, S. Tadesse, Y. Zhang, S. K. Pramanik, J.M. Wachira, S. Ghimire, P. McCarthy, A. Barfield, H.N. Banerjee, C. Chen, J.A. Golen, A.L. Rheingold, J.A. Krause, D.M. Ho, P.Y. Zavalij, R. Shaw, S.K. Mandal, Unprecedented anticancer activities of organorhenium sulfonato and carboxylato complexes against hormone-dependent MCF-7 and hormone-independent triple-negative MDA-MB-231 breast cancer cells, Mol. Cell. Biochem. 441 (2018) 151.
[62] E. Boros, P.J. Dyson, G. Gasser, Classification of metal-based drugs according to their mechanisms of action, Chem 6 (2020) 41.
[63] C.C. Musonda, J. Gut, P.J. Rosenthal, V. Yardley, R.C. Carvalho de Souza, K. Chibale, Application of multicomponent reactions to antimalarial drug discovery. Part 2: new antiplasmodial and antitrypanosomal 4-aminoquinoline γ- and δ-lactams via a 'catch and release' protocol, Bioorg. Med. Chem. 14 (2006) 5605.
[64] S.S. Maurya, A. Bahuguna, S.I. Khan, D. Kumar, R. Kholiya, D.S. Rawat, N-Substituted aminoquinoline-pyrimidine hybrids: synthesis, in vitro antimalarial activity evaluation and docking studies, Eur. J. Med. Chem. 162 (2019) 277.
[65] K. Wang, L. Huang, L. Gao, L. Jin, C. Huang, Synthesis, crystal structure, and photoelectric properties of Re(CO)3ClL (L = 2-(1-Ethylbenzimidazol-2-yl) pyridine), Inorg. Chem. 41 (2002) 3353.
[66] Á.D. Hernández Mejías, A. Poirot, M. Rmili, N. Leygue, M. Wolff, N. Saffon-Merceron, E. Benoist, S. Fery-Forgues, Efficient photorelease of carbon monoxide from a luminescent tricarbonyl rhenium(i) complex incorporating pyridyl-1,2,4-triazole and phosphine ligands, Dalton Trans. 50 (2021) 1313.
[67] S. Nasiri Sovari, I. Kolly, K. Schindler, Y. Cortat, S.-C. Liu, A. Crochet, A. Pavic, F. Zobi, Efficient direct nitrosylation of α-diimine rhenium tricarbonyl complexes to structurally nearly identical higher charge congeners activable towards photo-CO release, Molecules 26 (2021) 5302.
[68] (a) M. Wang, K. Murata, Y. Koike, G. Jonusauskas, A. Furet, D.M. Bassani, D. Saito, M. Kato, Y. Shimoda, K. Miyata, K. Onda, K. Ishii, A red-light-driven CO-releasing complex: photoreactivities and excited-state dynamics of highly distorted tricarbonyl rhenium phthalocyanines, Chem. Eur J. 28 (2022) e202200716;
(b) V.C. Weiss, G. Farias, A.L. Amorim, F.R. Xavier, T.P. Camargo, M.B. Bregalda, M. Haukka, E. Nordlander, B. de Souza, R.A. Peralta, Luminescent photoCORMs: enabling/disabling CO delivery upon blue light irradiation, Inorg. Chem. 59 (2020) 13078.
[69] D.R. Melis, C.B. Barnett, L. Wiesner, E. Nordlander, G.S. Smith, Quinoline-triazole half-sandwich iridium(iii) complexes: synthesis, antiplasmodial activity and preliminary transfer hydrogenation studies, Dalton Trans. 49 (2020) 11543.
[70] E. Bursal, F. Turkan, K. Buldurun, N. Turan, A. Aras, N. Çolak, M. Murahari, M. C. Yergeri, Transition metal complexes of a multidentate Schiff base ligand containing pyridine: synthesis, characterization, enzyme inhibitions, antioxidant properties, and molecular docking studies, Biometals 34 (2021) 393.
[71] E.M. Njogu, B. Omondi, V.O. Nyamori, Silver(I)-pyridinyl Schiff base complexes: synthesis, characterisation and antimicrobial studies, J. Mol. Struct. 1135 (2017) 118.
[72] A.K. Pramanik, M.S. Jana, S. Kundu, T.K. Mondal, Re(I) carbonyl complexes of N-[(2-pyridyl)methyliden]-α (or β)-aminonaphthalene: synthesis, structure, electrochemistry and DFT analysis, J. Mol. Struct. 1017 (2012) 19.
[73] X. Song, M.H. Lim, D.K.B. Mohamed, S.M. Wong, J. Zhao, T.S.A. Hor, Re(I) carbonyl complexes containing pyridyl-imine and amine ligands: synthesis, characterization and their catalytic olefin epoxidation activities, J. Organomet. Chem. 814 (2016) 1.
[74] R.S. Herrick, I. Wrona, N. McMicken, G. Jones, C.J. Ziegler, J. Shaw, Preparation and characterization of rhenium(I) compounds with amino ester derivatized diimine ligands. Investigations of luminescence. Crystal structures of Re(CO)3Cl (pyca-β-Ala-OEt) and Re(CO)3Cl(pyca-l-Asp(OMe)-OMe), J. Organomet. Chem. 689 (2004) 4848.
[75] L.A. Worl, R. Duesing, P. Chen, L.D. Ciana, T.J. Meyer, Photophysical properties of polypyridyl carbonyl complexes of rhenium(I), Dalton Trans. (1991) 849.
[76] L. Wallace, D.P. Rillema, Photophysical properties of rhenium(I) tricarbonyl complexes containing alkyl- and aryl-substituted phenanthrolines as ligands, Inorg. Chem. 32 (1993) 3836.
[77] G. Tapolsky, R. Duesing, T.J. Meyer, Synthetic control of excited-state properties in ligand-bridged complexes of rhenium(I). Intramolecular energy transfer by an electron-transfer/energy-transfer cascade, Inorg. Chem. 29 (1990) 2285.
[78] L. Sacksteder, A.P. Zipp, E.A. Brown, J. Streich, J.N. Demas, B.A. DeGraff, Luminescence studies of pyridine .alpha.-diimine rhenium(I) tricarbonyl complexes, Inorg. Chem. 29 (1990) 4335.
[79] L.D. Ramos, H.M. da Cruz, K.P. Morelli Frin, Photophysical properties of rhenium (i) complexes and photosensitized generation of singlet oxygen, Photochem. Photobiol. Sci. 16 (2017) 459.
[80] L. He, Z.-Y. Pan, W.-W. Qin, Y. Li, C.-P. Tan, Z.-W. Mao, Impairment of the autophagy-related lysosomal degradation pathway by an anticancer rhenium(i) complex, Dalton Trans. 48 (2019) 4398.
[81] G. Gasser, A. Pinto, S. Neumann, A.M. Sosniak, M. Seitz, K. Merz, R. Heumann, N. Metzler-Nolte, Synthesis, characterisation and bioimaging of a fluorescent rhenium-containing PNA bioconjugate, Dalton Trans. 41 (2012) 2304.
[82] B.L. Murphy, S.C. Marker, V.J. Lambert, J.J. Woods, S.N. MacMillan, J.J. Wilson, Synthesis, characterization, and biological properties of rhenium(I) tricarbonyl complexes bearing nitrogen-donor ligands, J. Organomet. Chem. 907 (2020) 121064.
[83] C.E. Housecroft, A.G. Sharpe, Inorganic Chemistry, fourth ed., Pearson, Harlow, England, 2012.
[84] N. Shavaleev, Z. Bell, G. Accorsi, M. Ward, Syntheses and structures of mononuclear {Re(CO) 3Cl(NN)} 'complex ligands' with a pendant imino–pyridine binding site, and preparation of some heterodinuclear Re(I)–lanthanide(III) complexes, Inorg. Chim. Acta. 351 (2003) 159.
[85] P. Kurz, B. Probst, B. Spingler, R. Alberto, Ligand variations in [ReX(diimine $(CO)_3$] complexes: effects on photocatalytic CO_2 reduction, Eur. J. Inorg. Chem. (2006) 2966, 2006.
[86] J.P. Jasinski, R.J. Butcher, A.N. Mayekar, H.S. Yathirajan, B. Narayana, B. K. Sarojini, Synthesis, crystal structures and theoretical studies of four Schiff

bases derived from 4-hydrazinyl-8-(trifluoromethyl) quinoline, J. Mol. Struct. 980 (2010) 172.
[87] S. Keller, Y.C. Ong, Y. Lin, K. Cariou, G. Gasser, A tutorial for the assessment of the stability of organometallic complexes in biological media, J. Organomet. Chem. 906 (2020) 121059.
[88] M.D. Hall, K.A. Telma, K.E. Chang, T.D. Lee, J.P. Madigan, J.R. Lloyd, I. S. Goldlust, J.D. Hoeschele, M.M. Gottesman, Say no to DMSO: dimethylsulfoxide inactivates cisplatin, carboplatin, and other platinum complexes, Cancer Res. 74 (2014) 3913.
[89] J. Karges, S. Kuang, Y.C. Ong, H. Chao, G. Gasser, One- and two-photon phototherapeutic effects of Ru(II) polypyridine complexes in the hypoxic centre of large multicellular tumor spheroids and tumor-bearing mice, Chemistry 27 (2021) 362.
[90] M. Patra, T. Joshi, V. Pierroz, K. Ingram, M. Kaiser, S. Ferrari, B. Spingler, J. Keiser, G. Gasser, DMSO-mediated ligand dissociation: renaissance for biological activity of N-heterocyclic-[Ru(η6-arene)Cl2] drug candidates, Chemistry 19 (2013) 14768.
[91] N. Summa, W. Schiessl, R. Puchta, N. van Eikema Hommes, R. van Eldik, Thermodynamic and kinetic studies on reactions of Pt(II) complexes with biologically relevant nucleophiles, Inorg. Chem. 45 (2006) 2948.
[92] Y.W. Yi, I. Bae, Effects of solvents on in vitro potencies of platinum compounds, DNA Repair 10 (2011) 1084.
[93] T. Mosmann, Rapid colorimetric assay for cellular growth and survival: application to proliferation and cytotoxicity assays, J. Immunol. Methods 65 (1983) 55.
[94] N. Nayeem, M. Contel, Exploring the potential of metallodrugs as chemotherapeutics for triple negative breast cancer, Chem. Eur J. 27 (2021) 8891.
[95] L.K. Diaz, V.L. Cryns, W.F. Symmans, N. Sneige, Triple negative breast carcinoma and the basal phenotype: from expression profiling to clinical practice, Adv. Anat. Pathol. 14 (2007) 419.
[96] V. Valdiglesias, S. Giunta, M. Fenech, M. Neri, S. Bonassi, γH2AX as a marker of DNA double strand breaks and genomic instability in human population studies, Mutat. Res. 753 (2013) 24.
[97] S. Gobeil, C.C. Boucher, D. Nadeau, G.G. Poirier, Characterization of the necrotic cleavage of poly(ADP-ribose) polymerase (PARP-1): implication of lysosomal proteases, Cell Death Differ. 8 (2001) 588.
[98] (a) M.N. Patel, H.N. Joshi, C.R. Patel, Cytotoxic, antibacterial, DNA interaction and superoxide dismutase like activities of sparfloxacin drug based copper(II) complexes with nitrogen donor ligands, Spectrochim. Acta Part A Mol. Biomol. Spectrosc. 104 (2013) 48;
(b) M. Dimitrakopolou, C. Dendrinou-Samara, A.A. Pantazaki, M. Alexiou, E. Nordlander, D. Kessissoglou, Interaction of tetranuclear [Mn4(II/II/II/IV)] mixed valence clusters with DNA, J. Inorg. Biochem. 102 (2008) 618.
[99] (a) A. Wolfe, G.H. Shimer Jr., T. Meehan, Polycyclic aromatic hydrocarbons physically intercalate into duplex regions of denatured DNA, Biochemistry 26 (1987) 6392;
(b) S. Nafisi, G.B. Sadeghi, A. PanahYab, Interaction of aspirin and vitamin C with bovine serum albumin, J. Photochem. Photobiol., B 105 (2011) 198–202.
[100] (a) A.A. Tikhomirova, N.A. Tcyrulnikov, R.M. Wilson, Synthesis, characterization, DNA binding and cleaving properties of photochemically activated phenanthrene dihydrodioxin, J. Photochem. Photobiol. Chem. 380 (2019) 111803;
(b) J.Q. Sha, X. Li, H.B. Qiu, Y.H. Zhang, H. Yan, Nickel complexes of the different quinolone antibacterial drugs: synthesis, structure and interaction with DNA, Inorg. Chim. Acta. 383 (2012) 178–184.
[101] (a) Y. Liu, K. Zhang, R. Lei, J. Liu, T. Zhou, Z.-Y. Yang, DNA-binding and anti-oxidation properties of binuclear lanthanide(III) complexes of 8-hydroxyquinoline-7-carbaldehyde-(isonicotinyl)hydrazone, J. Coord. Chem. 65 (2012) 2041;
(b) M. Anjomshoa, S.J. Fatemi, M. Torkzadeh-Mahani, H. Hadadzadeh, DNA-and BSA-binding studies and anticancer activity against human breast cancer cells (MCF-7) of the zinc (II) complex coordinated by 5, 6-diphenyl-3-(2-pyridyl)-1, 2, 4-triazine, Spectrochim. Acta Mol. Biomol. Spectrosc. 127 (2014) 511–520.
[102] A. Rescifina, C. Zagni, M.G. Varrica, V. Pistarà, A. Corsaro, Recent advances in small organic molecules as DNA intercalating agents: synthesis, activity, and modeling, Eur. J. Med. Chem. 74 (2014) 95.
[103] G. Balakrishnan, T. Rajendran, K. Senthil Murugan, M. Sathish Kumar, V. K. Sivasubramanian, M. Ganesan, A. Mahesh, T. Thirunalasundari, S. Rajagopal, Interaction of rhenium(I) complex carrying long alkyl chain with Calf Thymus DNA: cytotoxic and cell imaging studies, Inorg. Chim. Acta. 434 (2015) 51.
[104] M. Cory, D.D. McKee, J. Kagan, D.W. Henry, J.A. Miller, Design, synthesis, and DNA binding properties of bifunctional intercalators. Comparison of polymethylene and diphenyl ether chains connecting phenanthridine, J. Am. Chem. Soc. 107 (1985) 2528.
[105] M.J. Waring, Complex formation between ethidium bromide and nucleic acids, J. Mol. Biol. 13 (1965) 269.
[106] A.E. Friedman, C.V. Kumar, N.J. Turro, J.K. Barton, Luminescence of ruthenium (II) polypyridyls: evidence for intercalative binding to Z-DNA, Nucleic Acids Res. 19 (1991) 2595.
[107] M. Kaplanis, G. Stamatakis, V.D. Papakonstantinou, M. Paravatou-Petsotas, C. A. Demopoulos, C.A. Mitsopoulou, Re(I) tricarbonyl complex of 1,10-phenanthroline-5,6-dione: DNA binding, cytotoxicity, anti-inflammatory and anti-coagulant effects towards platelet activating factor, J. Inorg. Biochem. 135 (2014) 1.
[108] H.D. Stoeffler, N.B. Thornton, S.L. Temkin, K.S. Schanze, Unusual photophysics of a rhenium (I) dipyridophenazine complex in homogeneous solution and bound to DNA, J. Am. Chem. Soc. 117 (1995) 7119.
[109] V. Wing-Wah Yam, V. Wing-Man Lee, K.-K. Cheung, Synthesis, electrochemistry and photophysics of ruthenium(II) diimine complexes of 1,1′-bis (diphenylphosphino)ferrocene (dppf). Crystal structure of [Ru(bipy)2(dppf)]2+ (bipy = 2,2′-bipyridine), Dalton Trans. (1997) 2335.
[110] C.-C. Pagoni, V.-S. Xylouri, G.C. Kaiafas, M. Lazou, G. Bompola, E. Tsoukas, L. C. Papadopoulou, G. Psomas, D. Papagiannopoulou, Organometallic rhenium tricarbonyl–enrofloxacin and –levofloxacin complexes: synthesis, albumin-binding, DNA-interaction and cell viability studies, J. Biol. Inorg. Chem. 24 (2019) 609.
[111] F.L. Thorp-Greenwood, M.P. Coogan, L. Mishra, N. Kumari, G. Rai, S. Saripella, The importance of cellular localisation of probes: synthesis, photophysical properties, DNA interactions and cellular imaging properties of rhenium dppz complexes with known cellular localisation vectors, New J. Chem. 36 (2012) 64.
[112] A. Heydari, H. Mansouri-Torshizi, Design, synthesis, characterization, cytotoxicity, molecular docking and analysis of binding interactions of novel acetylacetonatopalladium(ii) alanine and valine complexes with CT-DNA and BSA, RSC Adv. 6 (2016) 96121.
[113] P.D. Ross, S. Subramanian, Thermodynamics of protein association reactions: forces contributing to stability, Biochemistry 20 (1981) 3096.
[114] A. Alonso, M.J. Almendral, Y. Curto, J.J. Criado, E. Rodríguez, J.L. Manzano, Determination of the DNA-binding characteristics of ethidium bromide, proflavine, and cisplatin by flow injection analysis: usefulness in studies on antitumor drugs, Anal. Biochem. 355 (2006) 157.
[115] J.D. Shepherd, M.J. Fritzler, J.I. Watson, J.H. van de Sande, The binding of anti-DNA antibodies as measured fluorometrically by ethidium bromide, J. Rheumatol. 5 (1978) 391.
[116] A.S. Dorafshan Tabatabai, E. Dehghanian, H. Mansouri-Torshizi, Exploring the interaction between the newly designed antitumor Zn(II) complex and CT-DNA/BSA: spectroscopic methods, DFT computational analysis, and docking simulation, Appl. Biochem. Biotechnol. 195 (2023) 6276.
[117] L. Zarei, Z. Asadi, E. Samolova, M. Dusek, Z. Amirghofran, Pyrazolate as bridging ligand in stabilization of self-assemble Cu(II) Schiff base complexes: synthesis, structural investigations, DNA/protein (BSA) binding and growth inhibitory effects on the MCF7, CT-26, MDA-MB-231 cell lines, Inorg. Chim. Acta. 509 (2020) 119674.
[118] M.H. Gehlen, The centenary of the Stern-Volmer equation of fluorescence quenching: from the single line plot to the SV quenching map, J. Photochem. Photobiol. C Photochem. Rev. 42 (2020) 100338.
[119] D. İnci, R. Aydın, Y. Zorlu, Cu(ii) complex with auxin (3-indoleacetic acid) and an aromatic planar ligand: synthesis, crystal structure, biomolecular interactions and radical scavenging activity, Eur. Biophys. J. 50 (2021) 771.
[120] J.R. Lakowicz, G. Weber, Quenching of fluorescence by oxygen. Probe for structural fluctuations in macromolecules, Biochemistry 12 (1973) 4161.
[121] B.H.M. Hussein, Spectroscopic studies of 7, 8-dihydroxy-4-methylcoumarin and its interaction with bovine serum albumin, J. Lumin. 131 (2011) 900.
[122] S.M.T. Shaikh, J. Seetharamappa, P.B. Kandagal, D.H. Manjunatha, In vitro study on the binding of anti-coagulant vitamin to bovine serum albumin and the influence of toxic ions and common ions on binding, Int. J. Biol. Macromol. 41 (2007) 81.
[123] M.B. Ismail, I.N. Booysen, M.P. Akerman, DNA interaction studies of rhenium compounds with Schiff base chelates encompassing biologically relevant moieties, Nucleos. Nucleot. Nucl. 38 (2019) 950.
[124] I. Maisuls, F.M. Cabrerizo, P.M. David-Gara, B. Epe, G.T. Ruiz, DNA oxidation photoinduced by norharmane rhenium(I) polypyridyl complexes: effect of the bidentate N,N′-Ligands on the damage profile, Chem. Eur J. 24 (2018) 12902.
[125] J. Chellappa, S.T. David, R. Bennie, S. Abraham, S. Pillai, S. Sathyasheeli, Spectral, Electrochemical and DNA binding properties of some Macroacyclic Transition metal complexes using diverse spectral methods, Int. J. Res. Inorg. Chem. 5 (2015) 14.
[126] M. Shamsi, S. Yadav, F. Arjmand, Synthesis and characterization of new transition metal {Cu(II), Ni(II) and Co(II)} l-phenylalanine–DACH conjugate complexes: in vitro DNA binding, cleavage and molecular docking studies, J. Photochem. Photobiol. B Biol. 136 (2014) 1.
[127] R. Maier, M.R. Fries, C. Buchholz, F. Zhang, F. Schreiber, Human versus bovine serum albumin: a subtle difference in hydrophobicity leads to large differences in bulk and interface behavior, Cryst. Growth Des. 21 (2021) 5451.
[128] F. Mohammadlou, H. Mansouri-Torshizi, E. Dehghanian, M. Eslami-Moghadam, M. Dusek, V. Eigner, A new zinc(II) complex of 2-benzoimidazoledisulfide ligand: synthesis, X-ray crystallographic structure, investigation of CT-DNA and BSA interaction by spectroscopic techniques and molecular docking, J. Photochem. Photobiol. Chem. 443 (2023) 114830.
[129] D. Senthil Raja, G. Paramaguru, N.S.P. Bhuvanesh, J.H. Reibenspies, R. Renganathan, K. Natarajan, Effect of terminal N-substitution in 2-oxo-1,2-dihydroquinoline-3-carbaldehyde thiosemicarbazones on the mode of coordination, structure, interaction with protein, radical scavenging and cytotoxic activity of copper(ii) complexes, Dalton Trans. 40 (2011) 4548.
[130] K. Liu, H. Yan, G. Chang, Z. Li, M. Niu, M. Hong, Organotin(IV) complexes derived from hydrazone Schiff base: synthesis, crystal structure, in vitro cytotoxicity and DNA/BSA interactions, Inorg. Chim. Acta. 464 (2017) 137.
[131] S.S. Bhat, A.A. Kumbhar, H. Heptullah, A.A. Khan, V.V. Gobre, S.P. Gejji, V. G. Puranik, Synthesis, electronic structure, DNA and protein binding, DNA cleavage, and anticancer activity of fluorophore-labeled copper(II) complexes, Inorg. Chem. 50 (2011) 545.

[132] D.M. Poloni, O. Dangles, J.A. Vinson, Binding of plant polyphenols to serum albumin and LDL: healthy implications for heart disease, J. Agric. Food Chem. 67 (2019) 9139.
[133] T.E. Kydonaki, E. Tsoukas, F. Mendes, A.G. Hatzidimitriou, A. Paulo, L. C. Papadopoulou, D. Papagiannopoulou, G. Psomas, Synthesis, characterization and biological evaluation of (99m)Tc/Re-tricarbonyl quinolone complexes, J. Inorg. Biochem. 160 (2016) 94.
[134] G. Balakrishnan, T. Rajendran, K.S. Murugan, M. Ganesan, V.K. Sivasubramanian, S. Rajagopal, Synthesis, photophysics and the binding studies of rhenium(I) diimine surfactant complexes with serum albumins: a spectroscopic and docking study approach, J. Lumin. 205 (2019) 51.
[135] L. Fetzer, B. Boff, M. Ali, M. Xiangjun, J.-P. Collin, C. Sirlin, C. Gaiddon, M. Pfeffer, Library of second-generation cycloruthenated compounds and evaluation of their biological properties as potential anticancer drugs: passing the nanomolar barrier, Dalton Trans. 40 (2011) 8869.
[136] SAINT, Bruker AXS Inc., Madison, WI, USA, v.2019.1-0.
[137] G.M. Sheldrick, SHELXS-97, SHELXL-2014 and SADABS, A short history of SHELX, Acta Crystallogr. C71 (1997) 3–8.
[138] L.J. Barbour, X-seed — a software tool for supramolecular crystallography, J. Supramol. Chem. 1 (2001) 189.
[139] J.L. Atwood, L.J. Barbour, Molecular graphics: from science to art, Cryst. Growth Des. 3 (2003) 3.
[140] P.o.V.P. Ltd., Persistence of Vision Raytracer, 2014 retrieved from, Version 3.6. http://www.povray.org/download/.
[141] M.V. Berridge, A.S. Tan, Characterization of the cellular reduction of 3-(4,5-dimethylthiazol-2-yl)-2,5-diphenyltetrazolium bromide (MTT): subcellular localization, substrate dependence, and involvement of mitochondrial electron transport in MTT reduction, Arch. Biochem. Biophys. 303 (1993) 474.
[142] A. Welsh, L.I. Rylands, V.B. Arion, S. Prince, G.S. Smith, Synthesis and antiproliferative activity of benzimidazole-based, trinuclear neutral cyclometallated and cationic, N^N-chelated ruthenium(ii) complexes, Dalton Trans. 49 (2020) 1143.
[143] J.S. Bleloch, A. du Toit, L. Gibhard, S. Kimani, R.D. Ballim, M. Lee, A. Blanckenberg, S. Mapolie, L. Wiesner, B. Loos, S. Prince, The palladacycle complex AJ-5 induces apoptotic cell death while reducing autophagic flux in rhabdomyosarcoma cells, Cell Death Dis. 5 (2019) 60.
[144] C. Parker, W. Rees, Fluorescence spectrometry. A review, Analyst 87 (1962) 83–111.
[145] O. Trott, A.J. Olson, AutoDock Vina: improving the speed and accuracy of docking with a new scoring function, efficient optimization, and multithreading, J. Comput. Chem. 31 (2010) 455.